

Spatial and temporal variability of iodine in aerosol

Juan Carlos Gomez Martin¹, Alfonso Saiz-Lopez², Carlos Alberto Cuevas², Rafael Pedro Fernandez³, Benjamin Silas Gilfedder⁴, Rolf Weller⁵, Alex R. Baker⁶, Elise Droste⁶, and Senchao Lai⁷

¹Instituto de Astrofísica de Andalucía

²Spanish National Research Council (CSIC)

³National Research Council (CONICET)

⁴Universtiy of Bayreuth

⁵Alfred-Wegener-Institute

⁶University of East Anglia

⁷South China University of Technology

November 24, 2022

Abstract

In this work we describe the compilation and homogenization of an extensive dataset of aerosol iodine field observations in the period between 1963 and 2018 and we discuss the spatial and temporal dependences of total iodine in bulk aerosol by comparing the observations with CAM-Chem model simulations. Total iodine in aerosol shows a distinct latitudinal dependence, with an enhancement towards the northern hemisphere (NH) tropics and lower values towards the poles. This behavior, which has been predicted by atmospheric models to depend on the global distribution of the main oceanic iodine source (which in turn depends on the reaction of surface ozone with aqueous iodide on the sea water-air interface, generating gas-phase I_2 and HOI), is confirmed here by field observations for the first time. Longitudinally, there is some indication of a wave-one profile in the Tropics, which peaks in the Atlantic and shows a minimum in the Pacific, following the wave-one longitudinal variation of tropical tropospheric ozone. New data from Antarctica show that the south polar seasonal variation of iodine in aerosol mirrors that observed previously in the Arctic, with two equinoctial maxima and the dominant maximum occurring in spring. While no clear seasonal variability is observed in NH middle latitudes, there is an indication of different seasonal cycles in the NH tropical Atlantic and Pacific. A weak positive long-term trend is observed in the tropical annual averages, which is consistent with an enhancement of the anthropogenic ozone-driven global oceanic source of iodine over the last 50 years.

Spatial and temporal variability of iodine in aerosol

Juan Carlos Gómez Martín^{1*}, Alfonso Saiz-Lopez^{2*}, Carlos A. Cuevas², Rafael P. Fernandez³, Benjamin Gilfedder⁴, Rolf Weller⁵, Alex R. Baker⁶, Elise Droste^{6,7} and Senchao Lai⁸.

¹ Instituto de Astrofísica de Andalucía, CSIC, 18008, Granada, Spain

² Department of Atmospheric Chemistry and Climate, Institute of Physical Chemistry Rocasolano, CSIC, Serrano 119, 28006 Madrid, Spain

³ Institute for Interdisciplinary Science, National Research Council (ICB-CONICET), FCEN-UNCuyo, Mendoza, 5501, Argentina

⁴ Limnological Research Station, University of Bayreuth, Germany

⁵ Alfred-Wegener-Institut Helmholtz Zentrum für Polar- und Meeresforschung, Bremerhaven, Germany

⁶ Centre for Ocean and Atmospheric Science, School of Environmental Sciences, University of East Anglia, Norwich, UK

⁷ Department of Environmental Sciences, Wageningen University and Research Centre, Wageningen, Netherlands

⁸ South China University of Technology, School of Environment and Energy, Higher Education Mega Center, Guangzhou 510006, P.R. China

Correspondence to: jcgomez@iaa.es (Juan Carlos Gomez Martin), a.saiz@csic.es (Alfonso Saiz-Lopez)

Abstract

In this work we describe the compilation and homogenization of an extensive dataset of aerosol iodine field observations in the period between 1963 and 2018 and we discuss the spatial and temporal dependences of total iodine in bulk aerosol by comparing the observations with CAM-Chem model simulations. Total iodine in aerosol shows a distinct latitudinal dependence, with an enhancement towards the northern hemisphere (NH) tropics and lower values towards the poles. This behavior, which has been predicted by atmospheric models to depend on the global distribution of the main oceanic iodine source (which in turn depends on the reaction of surface ozone with aqueous iodide on the sea water-air interface, generating gas-phase I₂ and HOI), is confirmed here by field observations for the first time. Longitudinally, there is some indication of a wave-one profile in the Tropics, which peaks in the Atlantic and shows a minimum in the Pacific, following the wave-one longitudinal variation of tropical tropospheric ozone. New data from Antarctica show that the south polar seasonal variation of iodine in aerosol mirrors that observed previously in the Arctic, with two equinoctial maxima and the dominant maximum occurring in spring. While no clear seasonal variability is observed in NH middle latitudes, there is an indication of different seasonal cycles in the NH tropical Atlantic and Pacific. A weak positive long-term trend is observed in the tropical annual averages, which is consistent with an enhancement of the anthropogenic ozone-driven global oceanic source of iodine over the last 50 years.

1. Introduction

Iodine is a key element in mammalian metabolism whose major global source is oceanic surface gas

emissions of iodine-bearing molecules to the atmosphere [Whitehead, 1984]. The photooxidation of these compounds leads to chemical cycles that impact the oxidative capacity of the atmosphere, and to the partitioning of the iodine load to aerosol [Saiz-Lopez *et al.*, 2012a], which is the main carrier of this element towards continental food chains [Whitehead, 1984]. Even though the enrichment of marine aerosol in iodine is well established (I/Na ratio several hundred times that of bulk seawater) and has been documented in early works on atmospheric iodine chemistry (see Duce *et al.* [1965] and references therein), the specific processes controlling the phase-partitioning remain unknown. Uptake of gas-phase iodine compounds on sea-salt aerosol is believed to be responsible for this large enrichment [Duce *et al.*, 1983]. This, however, is not an irreversible sink for iodine, since chemical processes analogous to those leading to the release of iodine-bearing gases from the sea surface [Miyake and Tsunogai, 1963; Garland and Curtis, 1981; Carpenter *et al.*, 2013; MacDonald *et al.*, 2014] occur as well on air-aqueous aerosol interfaces [Magi *et al.*, 1997].

Iodine in aerosol has received less attention than gas-phase iodine and its chemistry remains poorly understood [Saiz-Lopez *et al.*, 2012a]. Uptake of iodine oxides (I_xO_y) and oxyacids (HOI_x), as well as of iodine nitrate ($IONO_2$) and nitrite ($IONO$) on aerosol surfaces remains to be studied more thoroughly both experimentally and theoretically. The processing and partitioning between water insoluble and soluble iodine species, between soluble organic and inorganic iodine, and in the latter group between aqueous iodide (I^-) and iodate (IO_3^-), are essentially unknown. This includes the formation of volatile species that can go back to the gas phase (recycling), which is thought to occur via I^- , and the formation of species assumed to be stable and unreactive, i.e. iodate IO_3^- [Vogt *et al.*, 1999]. The existing aerosol chemical schemes cannot explain the speciation variability and the relative concentrations of iodide and iodate observed in the field. The aerosol I^- concentration is predicted to be negligible as a result of recycling to the gas phase, while IO_3^- is predicted to accumulate in particles [Vogt *et al.*, 1999; Pechtl *et al.*, 2007]. However many field observations show a significant I^- concentration in aerosol samples [Gäbler and Heumann, 1993; Wimschneider and Heumann, 1995; Baker, 2004; Baker, 2005; Lai *et al.*, 2008; Yu *et al.*, 2019].

Despite the many existing unknowns about aerosol iodine chemistry and speciation, the total iodine (TI) content of aerosol can be expected to gauge the strength of the iodine oceanic emissions and thus provide a sense of how these vary with location and time. Currently, the major source of iodinated gases to the troposphere is believed to be the reaction of gas-phase O_3 with I^- on the seawater-air interface. This assessment is mainly based on laboratory work [Garland and Curtis, 1981; Carpenter *et al.*, 2013; MacDonald *et al.*, 2014], and the ability of global models to reproduce the observations of gas-phase iodine monoxide (IO) at a few locations [Saiz-Lopez *et al.*, 2014; Sherwen *et al.*, 2016b]. In addition, Sherwen *et al.* [2016a] used a set of TI and total soluble iodine (TSI) open ocean observations to test the performance of global simulations of tropospheric iodine aerosol with GEOS-Chem, obtaining broad agreement with the relatively sparse cruise data considered. These simulations

predict the highest TI to occur in the tropical marine boundary layer (MBL), as a result of the latitudinal dependence of iodine gas source emissions [Prados-Roman *et al.*, 2015a] that results from the superposition of the seawater I⁻ and gas-phase O₃ distributions.

A wealth of field observations of TI in bulk aerosol and fine and coarse aerosol, as well as of iodine speciation exist (Figure 1). These results, however, are scattered in the literature and no attempt of putting together a comprehensive database and investigating its spatial and temporal variability has been carried out to the best of our knowledge. A list of total iodine and soluble iodine speciation observations was compiled for a previous review of atmospheric iodine chemistry [Saiz-Lopez *et al.*, 2012a], but some important historic datasets were missed (e.g. all the PEM WEST A results), and new cruise and ground-based observations are currently available. There are reasons to exclude TI observations at coastal and island stations from a comparison with global simulations, e.g. observations may be biased by locally intensive biogenic emissions with respect to oceanic observations, which are sensitive to less intensive but more widespread sources of iodine. However, the sparsity of the cruise data and its concentration mostly in the Atlantic suggests resorting to the abundant data obtained from ground-based stations.

The present paper deals with the compilation of a global aerosol TI dataset including both cruise and ground-based (coastal and insular) observations and the analysis of its spatial and temporal trends. The dataset includes unpublished aerosol iodine data obtained from the analysis of samples collected at Neumayer II Station (Antarctica) [Weller *et al.*, 2008] and during a short cruise around the island of Monserrat in the Tropical Atlantic [Lin *et al.*, 2016], as well as data obtained in three cruises that have only been fully reported in two PhD theses and a MSc thesis [Lai, 2008; Yodle, 2015; Droste, 2017], and an improved analysis and extended version of the TI data of the 23rd Chinese Antarctic Campaign cruise [Lai *et al.*, 2008; Gilfedder *et al.*, 2010]. CAM-Chem global simulations are then employed to test the performance of the model in reproducing these trends and distributions, with the purpose of highlighting the existing uncertainties and/or the importance of including missing processes in global simulations. Iodine partitioning between coarse and fine aerosol and speciation will be discussed in a follow up publication. A spreadsheet containing the compiled data can be found in the Supplementary Information.

2. Methods

2.1. Definitions

The TI concentration (in pmol m⁻³) is defined as the amount of particulate iodine collected by a filter or collection surface per volume unit of sampled air. Extraction methods may use a solvent (usually water) to facilitate the analysis. Thus, TI is the sum of total water-soluble iodine (TSI) plus non-soluble iodine (NSI), i.e. $TI = TSI + NSI$. TSI comprises total inorganic iodine ($TII = I^- + IO_3^-$) and soluble organic iodine (SOI), i.e.: $TSI = TII + SOI$. Total gas-phase iodine (TI_y) consist of the sum of gas-phase organic iodine (GOI) and inorganic iodine (IO_y) in the gas phase, i.e.: $TI_y = GOI + IO_y$.

Table 1 lists the acronyms used throughout this work and the corresponding definitions.

Aerosol size-segregated observations of TI and/or TSI have been reported by means of set of stacked filters or by using cascade impactors (CI) [Duce *et al.*, 1965; Duce *et al.*, 1967; Gilfedder *et al.*, 2008]. The bulk TI concentration is the sum of the TI within each size range. Usually, aerosol TI is reported for coarse (diameter $d > 1 \mu\text{m}$) and fine ($d < 1 \mu\text{m}$) aerosol, and $\text{TI}_{\text{bulk}} = \text{TI}_{\text{fine}} + \text{TI}_{\text{coarse}}$. There are however other studies where TI in particulate matter with $d \leq 2.5 \mu\text{m}$ ($\text{PM}_{2.5}$) collected by virtual impactors (VI) is reported [Gilfedder *et al.*, 2008]. When collecting filters are used, typical extraction procedures include thermal extraction, ultrasonication, and mechanical shaking [Yodle and Baker, 2019]. In combination with these methods for measuring TI in aerosol, techniques for capturing gas-phase IO_y and TI_y have also been implemented. For IO_y , the air flow may be passed additionally through filters impregnated in alkaline substances [Rancher and Kritz, 1980; Gäbler and Heumann, 1993] or bubbled through an alkaline solution [Duce *et al.*, 1965]. For TI_y , a combination of an electrostatic precipitator and a charcoal trap has been used [Moyers and Duce, 1972; 1974]. A more modern method for determining the concentration of iodocarbons is Gas Chromatography-Mass Spectrometry (GC-MS) analysis of air samples stored in canisters, but it does not appear to have been applied to measure the overall airborne iodine budget.

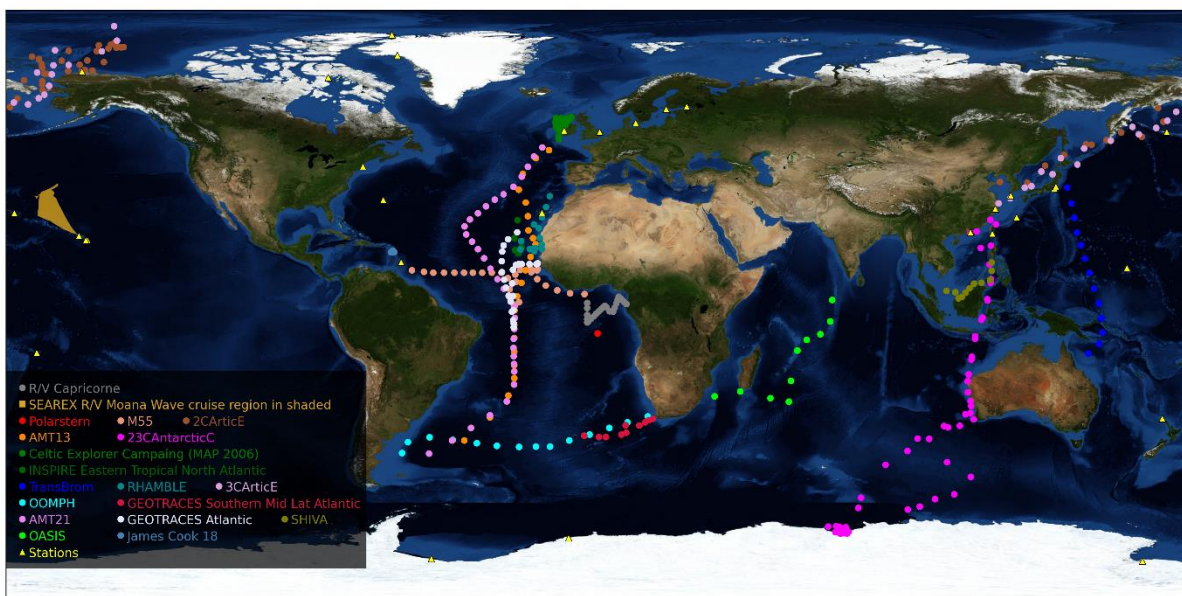


Figure 1. Geographical distribution of total iodine (TI) and total soluble iodine (TSI) observations. Stations: Yellow triangles; Cruises: colour-coded dots (see legend). The SEAREX cruise region is shown in shaded, because the aerosol sampling points are not available (only the average TI for the second leg of the cruise was reported).

The analytical method most widely used to quantify TI in older observations is Instrumental Neutron Activation Analysis (INAA) (e.g. [Duce *et al.*, 1965; Duce *et al.*, 1973; Arimoto *et al.*, 1989; Arimoto *et al.*, 1996]). Isotope Dilution Mass Spectrometry (IDMS) has also been used to determine TI [Gäbler and Heumann, 1993]. Contemporary observations employ more accessible techniques such as Thermal Extraction with Spectrometric detection of Iodine (TESI) [Gilfedder *et al.*, 2010] for TI and

Inductively Coupled Plasma-Mass Spectrometry (ICP-MS) for TSI (e.g. [Baker, 2005; Lai et al., 2008]).

Table 1. Definition of iodine variables

Acronym/symbol	Definition
TI	Total iodine (in aerosol)
NSI	Non-soluble iodine (in aerosol)
TSI	Total soluble iodine (in aerosol)
TII	Total inorganic iodine (in aerosol)
SOI	Soluble organic iodine (in aerosol)
$X_{\text{bulk}}, X_{\text{fine}}, X_{\text{coarse}}$ ($X = \text{TI}, \text{TSI}, \text{etc.}$)	Iodine in bulk aerosol, in the fine aerosol fraction and in the coarse aerosol fraction, respectively
$\text{TI}_x, \text{TSI}_x$	TI and TSI for $d < x \mu\text{m}$
TI_v	Total iodine (gas-phase)
IO_v	Inorganic iodine (gas phase)
GOI	Gas-phase organic iodine

2.2. Description and treatment of published datasets

2.2.1. Geographical distribution

We have compiled iodine aerosol data from 55 field campaigns across the globe spanning 55 years (1963 to 2018), consisting of 7794 datapoints (Supplementary Information). Of these, 7722 are measurements of individual samples and the remaining 22 points are the reported averages of a total of 510 samples which we have not been able to retrieve. Since the source of iodine is mainly marine, only ship-borne, coastal or insular campaigns have been considered. Tables 1 and 2 list the 19 cruises (C#) and 36 coastal ground-based (S#) campaigns where aerosol iodine measurements have been carried out. Figure 1 shows the geographical distribution of these observations. The dataset samples well the latitudinal coordinate. Longitudinally, most observations are concentrated in the Atlantic, while there is a complete lack of data in the Eastern Pacific.

Some locations need to be considered carefully, since they may be affected by locally enhanced sources of iodine. For example, there is evidence that the MAP 2006 [Gjlfedder et al., 2008; Lai, 2008] data (S32) is affected by intense particle formation following biogenic emissions. Similarly, the decline of Arctic sea ice may have enhanced airborne iodine in C13 with respect to C7 [Kang et al., 2015]. Also, aerosol sampled in the free troposphere (S1c, S1d, S7, S17) is likely to show different iodine content than at sea level.

2.2.2. Types of data

Most of the samples were analyzed for TI, but in some of the recent works TSI analysis was reported (C4, C6, C8, C9, C10, C14, C17, C18, C19, S32, S36). Fortunately, the samples of some cruises (C5, C7, C11, C12, C13) and ground-based campaigns (S14, S34, S35) were analyzed for both TI and TSI, which allows obtaining a relationship between both quantities to convert TSI into TI (see Section 3.1). Similarly, most works report bulk aerosol measurements. Only two cruises (C8 and C9) reported exclusively $\text{PM}_{2.5}$ measurements. Again, CI size-segregated data is available for several campaigns

(S1, S2, S4, S9, S20, S32), which enables to deduce a relationship between $TI_{2-2.5}$ and TI_{bulk} . Regarding gas-phase measurements, campaigns C1, S1, S5, S6 and S29 report measurements of IO_y or TI_y .

2.2.3. Quality of data

Sample data availability. In some cases, the individual sample data (C3, S8, S10, S28 and S29) are plotted in the original publication, but no longer available or not accessible in digital form. In these cases, the data has been digitized from the plots in the original papers. In newer publications, digitization of plots with many datapoints can be done with good accuracy (e.g. S28), but in older papers this is not always the case. For the Mould Bay (S8) and Igloolik (S10) stations, the data are affected by the clustering of the symbols in the plot and some points may be missing because of fading symbols in the hard copy from which the papers were scanned. Thus, the number of samples and the actual values may differ from the original data, although the overall campaign statistics are close to those of the original data.

Only campaign statistics reported. Comparing cruise and ground-based measurements is often difficult, since cruise observations are snapshots of the state of the atmosphere, while ground-based observations enable much longer integration times. Some papers report only statistics of long-term sampling, and do not provide the individual measurements (C2, S7, S12, S13, S20, S30 and S36). Moreover, the statistics provided in different works may differ (e.g. for S12 the geometric mean is reported instead of the arithmetic mean). This may cause a problem of consistency in the treatment of the full dataset. In the present paper we use the arithmetic mean and we have estimated it if not available.

Data below detection limit. We are aware of a campaign in coastal Australia (MUMBA) where TI measurements with ion beam analysis – particle induced x-ray emission (IBA-PIXE) were carried out [Paton-Walsh et al., 2017]. The concentrations determined were below a detection limit of ~ 1.2 nmol m^{-3} (Perry Davy, personal communication), which is two orders of magnitude higher than typical TI concentrations measured in the same region (~ 10 pmol m^{-3} , campaigns S12 and S13). Thus, we are unable to use this dataset.

2.3. Collection and analysis of datasets reported for the first time

2.3.1. Neumayer II

We include in our data compilation an unpublished TSI dataset (S33) obtained from a ground-based campaign at Neumayer II Station (Antarctica). The samples were collected over one year (January 2007 to January 2008), and thus enable to inspect the seasonal variation of aerosol iodine at an Antarctic location in full for the first time. A description of the sampling technique and the conditions at the Neumayer station during sampling can be found in Weller et al. [2008]. Briefly, the aerosol samples were collected on pre-cleaned Whatman 541 filters at a flow rate of 120 m^3 h^{-1} . Each sample

was composed of two filters in series using a ventilated electropolished stainless steel inlet stack (total height about 8 m above the snow surface), with a 50% aerodynamic cut-off at diameter around 7–10 μm at wind velocities between 4 and 10 m s^{-1} . Samples for TSI analysis were first extracted from a portion of each filter using 50 ml MilliQ water by first shaking and then followed by 15 min in an ultrasonic bath. Total iodine was measured using a quadrupole inductively coupled plasma-mass spectrometer (Perkin Elmer Elan) as in Gilfedder et al. [2007]. Rhenium was used as an internal standard, with the ICP-MS peak hopping on the ^{127}I and ^{187}Re isotopes. A new calibration was done every 20 samples. The accuracy of the method was checked by comparison with the international reference material BCR-611. The method has a detection limit around $7 \times 10^{-3} \text{ pmol m}^{-3}$.

2.3.2. RRS James Cook Cruise 18 (JC19)

JC18 was a UK NERC-funded short cruise around the island of Monserrat in the Tropical Atlantic-Caribbean Sea between 4th and 14th December 2007. The sample collection methods are described by [Lin et al., 2016]. Here we report fine and coarse measurements of TSI by ICP-MS and TI by INAA. The ICP-MS data were obtained using the same method as published in [Baker, 2005]. The INAA results were done by the same lab that produced the TI data from the GEOTRACES cruises D357 and D361 [Sherwen et al., 2016a].

2.3.3. Extended 23rd Chinese Antarctic Campaign TI dataset

The complete TSI dataset measured by ICP-MS and five TI datapoints measured by TESI from the Xue-Long cruise to Antarctica in 2005-2006 have been previously reported [Lai et al., 2008; Gilfedder et al., 2010]. Here, we report the complete TI dataset for the first time. Analytical methods are described in [Gilfedder et al., 2010]. New TI values were measured for all the samples in one run after optimization of the method following publication of the five TI data points by Gilfedder et al. [2010]. Although replicates could not be carried out for the full dataset due to the scarcity of filter paper, the precision is expected to be as good or better than in the earlier measurements as a result of accumulated experience and method optimization.

2.3.4. Celtic Explorer MAP 2006 cruise

Measurements of soluble iodine in two $\text{PM}_{2.5}$ samples (day- and nighttime) obtained during the Celtic Explorer cruise in June-July 2006 have been reported previously [Gilfedder et al., 2008]. Here we include the full dataset, which is part of a Senchao Lai's PhD thesis. The samples were collected on conventional fiber filters by using a VI, and analyzed by ICP-MS. Further details on the sampling and analytical methods can be found in [Lai, 2008].

2.3.5. RRS Discovery AMT21 cruise, and R/V Sonne OASIS and TransBrom cruises.

Aerosol samples were collected during the TransBrom cruise in the Western Pacific aboard R/V Sonne (SO202-2) between 10th and 22nd October 2009 [Martino et al., 2014]. Samples were also collected in the Tropical Indian Ocean aboard of the R/V Sonne (SO234-1/2) between 8th and 20th

July 2014 and 23rd and 7th August 2014 within the framework of the OASIS project. The Atlantic Meridional Transect (AMT21) was conducted by the RSS Discovery between 29th September and 14th November 2011. The sampling and analysis methods employed in the AMT21 and OASIS campaigns were identical (high volume air sampler, CI collection on glass microfiber filters, ICP-MS analysis). Whatman 41 cellulose filters were used instead on the TransBrom cruise. Further details can be found in the PhD thesis of Chan Yodle [Yodle, 2015] and the MSc thesis of Elise Droste [Droste, 2017].

2.4. Model description

The halogen version of the global 3-D chemistry-climate model CAM-Chem (Community Atmospheric Model with chemistry, version 4) [Fernandez *et al.*, 2014; Saiz-Lopez *et al.*, 2014] has been used to calculate the reactive and total gas-phase iodine budget. The model setup includes a state-of-the-art emissions inventory and chemistry scheme for halogens (chlorine, bromine and iodine) [Fernandez *et al.*, 2014; Saiz-Lopez *et al.*, 2014]. Briefly, the iodine chemical scheme includes an independent representation of dry and wet deposition for each inorganic gas-phase iodine species (I, I₂, IO, OIO, INO, INO₂, IONO₂, HI, HOI, I₂O₂, I₂O₃, I₂O₄, IBr, ICl), which are termed collectively as IO_y. The organic iodine sources from a top-down emission inventory [Ordóñez *et al.*, 2012] represent the oceanic emissions and photochemical breakdown of four iodocarbons (CH₃I, CH₂ICl, CH₂IBr, CH₂I₂), including a cyclic seasonal variation. Inorganic sources of iodine (HOI and I₂ emitted from the ocean surface) are based on laboratory studies of the oxidation of aqueous iodide by surface ozone reacting on the ocean's surface [Carpenter *et al.*, 2013; MacDonald *et al.*, 2014], and are computed on-line [Prados-Roman *et al.*, 2015a]. In this work we use the output from a REF-C1 model run used previously to simulate the evolution of iodine concentration in the RECAP ice core (coastal East Greenland) [Cuevas *et al.*, 2018]. CAM-Chem was configured with a horizontal resolution of 1.9° latitude by 2.5° longitude and 26 vertical levels from the surface to the stratosphere (~40 km). The model was run in free-running mode considering prescribed sea surface temperature fields and sea ice distributions from 1950 to 2010 [Tilmes *et al.*, 2016], which covers the major part of the time span of observations (1963 to 2018). Therefore, the model dynamics and transport represent the daily synoptic conditions of the observations, and allows the direct online coupling between the ocean, ice, and atmospheric modules during the 60 years of simulation. A land-mask filter (land fraction < 1.0) has been applied to all longitudinal and latitudinal averages from the model output, in order to account only for coastal and open ocean regions.

Note that the 1950-2010 REF-C1 simulation used for model validation did not include the recent implementation of iodine sources and heterogeneous recycling occurring within the polar regions, which strongly affect the total gas-phase IO_y burden within the Arctic and Antarctica. Indeed, the development of the halogen polar module within CAM-Chem has only been applied to present time conditions and is based on a seasonal sea-ice climatology representative of the 2000th decade. Thus, and for the sake of highlighting the large differences on the surface iodine mixing ratios when

additional polar sources and chemistry are considered, the perpetual 2000 CAM-Chem output from [Fernandez *et al.*, 2019] has also been used to evaluate the model performance at high latitudes.

Although a detailed treatment of uptake, recycling and loss of individual IO_y gas-phase species on sea-salt aerosol and ice-crystals is included in CAM-Chem [Saiz-Lopez *et al.*, 2014; Saiz-Lopez *et al.*, 2015], the model does not track the TI content in aerosol [Koenig *et al.*, 2020]. Note that the accumulation of iodine in aerosol depends on a number unknown or highly uncertain chemical processes that require further investigation, for example the redox chemistry that may enable interconversion between IO₃⁻ (currently believed to be a sink) and I⁻ (currently thought to lead to recycling of gas-phase iodine), or the role of organic iodinated compounds as I⁻ reservoirs [Saiz-Lopez *et al.*, 2012a]. Currently, models are essentially unable to explain the speciation of iodine in aerosol, and in particular iodide concentrations are ~2 orders of magnitude lower than observations [Pechtl *et al.*, 2007]. Since IO_y uptake on aerosol determines the partitioning of iodine between IO_y and TI, it is expected that both quantities show similar spatial and temporal trends. Therefore, in this work we have used the modeled IO_y to compare with the aerosol TI observations. In doing so, we have scaled the model IO_y abundance by the IO_y/TI and TI_y/TI ratios computed from all cruises and campaigns where both total gas-phase and aerosol iodine were measured, as described below in section 3.2. Two caveats to this comparison at high latitudes are that the polar module is not fully tested due to sparse gas phase iodine measurements (especially in the Arctic region), and that the iodine budget is controlled by heterogeneous recycling on ice and loss to iodine oxide particles (IOPs). The later process is not yet implemented in the polar module, and this may lead to a significant overestimation of gas phase iodine.

291 **Table 2. List of cruises reporting aerosol iodine ^a**

#	Program / Campaign	Cruise	Location	Min lon	Max lon	Min lat	Max lat	Date start	Date end	N	Type of data	Methods	Ref.
C1		R/V Capricorne	Equatorial Atlantic	-2.7	9.2	-5.2	2.7	30-05-77	12-06-77	24	TI (bulk), IO _y	INAA	[Rancher and Kritz, 1980]
C2	SEAREX	Westerlies, R/V Moana Wave	North Pacific	-170	-149	22	40	10-06-86	11-07-86	17	TI (bulk)	INAA	[Arimoto et al., 1989]
C3	Polarstern Campaigns	ANT-VII/5 (PS14), R/V Polarstern	Tropical Atlantic	-1	2	-11	-6	18-03-89	18-03-89	1	I, IO ₃ ⁻ (bulk)	IDMS	[Wimschneider and Heumann, 1995]
C4	German SOLAS	M55, R/V Meteor	Tropical Atlantic	-56.2	-3.5	0.1	11.3	15-10-02	13-11-02	28	TSI (fine + coarse)	CI ^b ; ICP-MS	[Baker, 2005]
C5	CHINARE	2 nd CHINARE, R/V Xue-long	Western Pacific-Arctic Ocean	121	-150	35.0	80.0	15-07-03	26-09-03	44	TI, TSI (bulk)	ICP-MS	[Kang et al., 2015]
C6	AMT	AMT13 RRS James Clark Ross	Atlantic Transect	-40.2	-14.3	-41.1	47.3	14-09-03	08-10-03	22	TSI (fine + coarse)	CI ^b ; ICP-MS	[Baker, 2005]
C7	CAC	23 rd CAC R/V Xue-Long	Western Pacific-Indian-Southern Ocean	70.8	122.0	-69.3	26.2	20-11-05	22-03-06	57	TI, TSI (bulk)	TESI, ICP-MS	[Lai et al., 2008; Gilfedder et al., 2010], This work
C8	MAP	CEC, R/V Celtic Explorer	North Atlantic	-12.3	-7.5	50.7	57.4	12-06-06	05-07-06	33	TSI (PM _{2.5})	VI; IC-ICP-MS	[Gilfedder et al., 2008; Lai, 2008]
C9	OOMPH	VT 88 R/V Marion Dufresne	Southern Atlantic	-59.2	15.8	-44.9	-33.7	20-01-07	02-02-07	14	TSI (PM _{2.5})	ICP-MS	[Lai et al., 2011]
C10	RHaMBLe	RRS Discovery D319	East Tropical Atlantic	-23.1	-14.1	16.6	33.3	22-05-07	05-06-07	14	TSI (fine + coarse)	CI ^b ; ICP-MS	[Allan et al., 2009]

C11	UK-SOLAS	INSPIRE RRS Discovery D325	Eastern Tropical North Atlantic	-25.0	-22.8	16.0	26.0	17-11-07	16-12-07	17	TI, TSI (bulk)	TESI	[Gilfedder <i>et al.</i> , 2010; Sherwen <i>et al.</i> , 2016a]
C12		RRS James Cook Cruise 18 (JC18)	Tropical Atlantic	-63	-62.5	16.2	16.7	04-12-07	14-12-07	8	TI, TSI (fine + coarse)	CI ^b ; ICP-MS	This work
C13	CHINARE	3 rd CHINARE, R/V Xue-long	Western Pacific-Arctic Ocean	122	-146	31.2	85.1	13-07-08	21-09-08	28	TI, TSI (bulk)	ICP-MS	[Xu <i>et al.</i> , 2010]
C14	TransBrom	R/V Sonne SO202-2	Tropical Western Pacific	143.7	154.5	-14.6	36.0	10-10-09	22-10-09	13	TSI (fine + coarse)	CI ^b ; ICP-MS	[Yodle, 2015]
C15	UK-GEOTRACES	RRS Discovery D357	Southern Atlantic	-3.6	17.3	-40.0	-34.5	18-10-10	19-11-10	11	TI (bulk)	INAA	[Sherwen <i>et al.</i> , 2016a]
C16	UK-GEOTRACES	RRS Discovery D361	Atlantic transect	-28.8	-17.8	-6.6	22.3	21-02-11	16-03-11	24	TI (bulk)	INAA	[Sherwen <i>et al.</i> , 2016a]
C17	AMT	AMT21 RRS Discovery D371	Atlantic Transect	-51.0	-16.4	-45.1	48.2	01-10-11	07-11-11	33	TSI (fine + coarse)	CI ^b ; ICP-MS	[Yodle, 2015]
C18	SHIVA	R/V Sonne SO218	Tropical Western Pacific	106.9	120.7	2.2	13.1	16-11-11	28-11-11	11	TSI (bulk)	ICP-MS	[Yodle and Baker, 2019]
C19	OASIS	R/V Sonne SO 234-2 and SO235	Tropical Indian Ocean	35.0	72.0	-29.8	1.7	08-07-14	07-08-14	10	TSI (fine + coarse)	CI ^b ; ICP-MS	[Droste, 2017]

292 ^a Abbreviations: SOLAS: Surface-Ocean / Lower Atmosphere Study; AMT: Atlantic Meridional Transect; CHINARE: China National Arctic Research Expedition; CAC: China Antarctic Campaign; MAP: Marine Aerosol Production from Natural Sources; OOMPH: Organics over the Ocean Modifying Particles in both Hemispheres; RHAMBLE: Reactive Halogens in the Marine Boundary Layer; SHIVA: Stratospheric Ozone: Halogen Impacts in a Varying Atmosphere; OASIS: Organic very short lived substances and their Air Sea Exchange from the Indian Ocean to the Stratosphere; CI: Cascade Impactor; VI: Virtual Impactor; INAA: Instrumental Neutron Activation Analysis; ICP-MS: Inductively Coupled Plasma-Mass Spectrometry; IDMS: Isotope Dilution Mass Spectrometry; TESI: Thermal extraction with spectrometric detection. ^b Cascade impactors were also used to achieve the coarse/fine separation, but they weren't used to achieve detailed size segregation.

299 **Table 3. Campaigns in coastal and island stations reporting aerosol iodine measurements**

#	Program / Campaign	Location	Lon	Lat	Date start	Date end	N	Type of data	Methods	Ref.
S1a		Hilo, Hawaii, USA	-155.1	19.9	27-05-63	18-06-63	5	TI (size-segregated), IO _y	CI; INAA	[Duce <i>et al.</i> , 1965]
S1b		Mauna Loa, Hawaii, USA (600 m)	-155.6	19.9	05-06-63	25-06-63	2			
S1c		Mauna Loa, Hawaii, USA (2000 m)	-155.6	19.9	05-06-63	25-06-63	1			
S1d		Mauna Loa, Hawaii, USA (3300 m)	-155.6	19.9	05-06-63	25-06-63	1			
S2		Cambridge, Massachusetts, USA	-71.1	42.4	31-10-64	14-11-64	10	TI (size-segregated)	CI; INAA	[Lininger <i>et al.</i> , 1966]
S3		Barrow, Alaska, USA	-156.8	71.3	20-01-65	28-01-65	23	TI (bulk)	INAA	[Duce <i>et al.</i> , 1966]
S4		Hilo, Hawaii, USA	-155.1	19.9	01-08-66	31-08-66	8	TI (size-segregated)	CI; INAA	[Duce <i>et al.</i> , 1967]
S5		Oahu, Hawaii, USA	-157.7	21.3	01-08-69	10-08-69	11	TI (bulk), TI _y	INAA	[Moyers and Duce, 1972]
S6		McMurdo, Antarctica	166.7	-77.8	08-11-70	12-12-70	19	TI (bulk), TI _y	INAA	[Duce <i>et al.</i> , 1973]
S7		Mauna Loa, Hawaii, USA (3300 m)	-155.6	19.9	01-02-79	31-05-85	287	TI (bulk)	INAA	[Zieman <i>et al.</i> , 1995]
S8	CAASN	Mould Bay, Canada	-119.3	76.2	11-04-79	20-05-82	135	TI (bulk)	INAA	[Sturges and Barrie, 1988]
S9	SEAREX	Enewetak, Marshall Islands	162.0	11.5	18-04-79	04-08-79	27	TI (size-segregated)	CI; INAA	[Duce <i>et al.</i> , 1983]
S10	CAASN	Igloolik, Canada	-81.7	69.4	29-10-79	16-05-82	110	TI (bulk)	INAA	[Sturges and Barrie, 1988]
S11	CAASN	Alert, Canada	-62.3	82.5	13-07-80	18-12-06	1234	TI (bulk)	INAA	[Sharma <i>et al.</i> , 2019]
S12a	SEAREX	American Samoa ISS	-170.6	-14.3	01-07-81	31-08-81	7	TI (bulk)	INAA	[Arimoto <i>et al.</i> , 1987]
S12b	SEAREX	American Samoa OSS	-170.6	-14.3	01-07-81	31-08-81	4	TI (bulk)	INAA	[Arimoto <i>et al.</i> , 1987]
S13	SEAREX	New Zealand	172.7	-34.4	01-05-83	31-08-83	11	TI (bulk)	INAA	[Arimoto <i>et al.</i> ,

										1990]
S14		Tokyo, Japan	139.8	35.7	14-07-83	23-03-84	9	TI, TSI (bulk)	INAA	[Hirofumi <i>et al.</i> , 1987]
S15	AEROCE	Tudor Hill, Bermuda, UK	-64.87	32.24	29-07-88	26-12-97	1308	TI (bulk)	INAA	[Arimoto <i>et al.</i> , 1995]
S16	AEROCE	Ragged Point, Barbados	-59.4	13.2	17-08-88	30-12-97	2750	TI (bulk)	INAA	[Arimoto <i>et al.</i> , 1995]
S17	AEROCE	Izaña, Tenerife, Spain (2360 m)	-16.5	28.3	17-06-89	28-12-97	905	TI (bulk)	INAA	[Arimoto <i>et al.</i> , 1995]
S18	AEROCE	Mace Head, Ireland	-9.73	53.3	07-08-89	15-08-94	436	TI (bulk)	INAA	[Huang <i>et al.</i> , 2001]
S19		Ibaraki, Japan	140.3	36.3	19-02-90	13-05-91	13	TI (bulk)	INAA	[Yoshida and Muramatsu, 1995]
S20a		Uto, Finland	21.4	59.8	29-04-91	12-05-91	35	TI (fine + coarse)	2 filters, INAA	[Jalkanen and Manninen, 1996]
S20b		Virolahti, Finland	27.7	60.6	10-06-91	30-06-91	35	TI (fine + coarse)		
S21	PEM West A	Midway Island	-177.4	28.2	27-05-91	02-12-91	12	TI (bulk)	INAA	[Arimoto <i>et al.</i> , 1996]
S22	PEM West A	Hong Kong, China	114.3	22.6	06-09-91	25-11-91	50	TI (bulk)	INAA	[Arimoto <i>et al.</i> , 1996]
S23	PEM West A	Ken-Ting; Taiwan	120.9	21.9	08-09-91	23-10-91	29	TI (bulk)	INAA	[Arimoto <i>et al.</i> , 1996]
S24	PEM West A	Okinawa, Japan	128.3	26.9	09-09-91	09-12-91	8	TI (bulk)	INAA	[Arimoto <i>et al.</i> , 1996]
S25	PEM West A	Cheju Island; Korea	126.48	33.52	10-09-91	02-10-91	6	TI (bulk)	INAA	[Arimoto <i>et al.</i> , 1996]
S26	PEM West A	Oahu, Hawaii, USA	-157.7	21.3	18-09-91	31-10-91	37	TI (bulk)	INAA	[Arimoto <i>et al.</i> , 1996]
S27	PEM West A	Shemya, Alaska, USA	174.1	52.9	19-09-91	31-10-91	15	TI (bulk)	INAA	[Arimoto <i>et al.</i> , 1996]
S28	PSE	Alert, Canada	-62.3	82.5	22-01-92	15-04-92	85	TI (fine + coarse)	VI; INAA	[Barrie <i>et al.</i> , 1994]
S29		Weddell Sea (Filchner Station)	-50.2	-77.1	30-01-92	10-02-92	2	TI (coarse), IO _y , GOI	IDMS	[Gäbler and Heumann, 1993]
S30		Hong Kong, China	114.2	22.3	01-04-95	30-04-96	114	TI (bulk)	INAA	[Cheng <i>et al.</i> , 2000]
S31		Weybourne, UK	1.1	52.9	08-08-96	21-10-97	16	TI (bulk and size-segregated)	CI; INAA	[Baker <i>et al.</i> , 2000]

S32	MAP	Mace Head, Ireland	-9.7	53.3	13-06-06	06-07-06	75	TSI (fine + coarse, PM _{2.5})	CI, VI; ICP-MS	[<i>Gilfedder et al.</i> , 2008; <i>Lai</i> , 2008]
S33		Neumayer II, Antarctica	-8.3	-70.7	08-01-07	28-01-08	56	TSI (bulk)	ICP-MS	This work
S34	MAP	Mace Head, Ireland	-9.7	53.3	18-06-07	02-07-07	3	TI, TSI (bulk)	TESI, INAA	[<i>Gilfedder et al.</i> , 2010]
S35		Riso, Denmark	12.1	55.693	02-04-11	11-12-14	8	TI, TSI (bulk)	ICP-MS	[<i>Zhang et al.</i> , 2016]
S36		Xiangshan Gulf, Zhejiang, China	121.8	29.5	11-02-18	11-05-18	3	TSI (fine and bulk)	Nano-MOUDI; LC-MS; ICP-MS	[<i>Yu et al.</i> , 2019]

300 Notes: SEAREX: Sea/Air Exchange; CAASN: Canadian Arctic Aerosol Sampling Network; PSE: Polar Sunrise Experiment; AEROCE: Atmospheric/Ocean Chemistry
 301 Experiment; PEM West A: Pacific Exploratory Mission - West-A; American Samoa data ISS: inside selected sector, OSS: outside selected sector. Dates in italics: the
 302 original paper does not report exact dates, only months or season. CI: Cascade Impactor; VI: Virtual Impactor, nano-MOUDI: Nano-Microorifice Uniform Deposit Impactor;
 303 INAA: Instrumental Neutron Activation Analysis; ICP-MS: Inductively Coupled Plasma-Mass Spectrometry; IDMS: Isotope Dilution Mass Spectrometry; LC-MS: Liquid
 304 Chromatography Mass Spectrometry; TESI: Thermal extraction with spectrometric detection.

3. Results

3.1. Homogenization of total iodine data

In order to study TI spatial and time dependencies, the data needs to be homogenized. The first step is to scale TSI to TI where TI measurements were not performed. This is especially critical for most of the recent cruise samples, for which only TSI was measured (C4, C6, C8, C9, C10, C14, C17, C18, C19, C32, C36, S33). Similarly, measurements of fine particulate matter or $PM_{2.5}$ (C8 and C9) need to be scaled to make them directly comparable to bulk aerosol measurements.

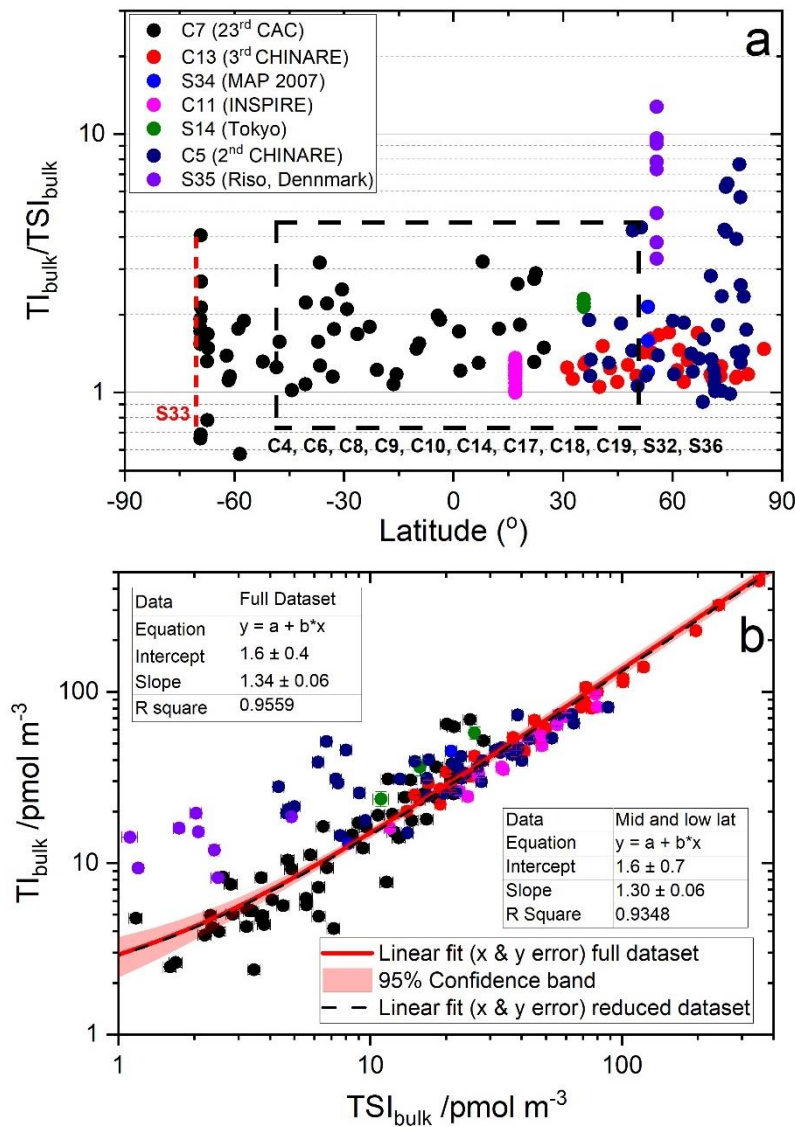


Figure 2. Correlation between total iodine (TI) and total soluble iodine (TSI). Panel a: observed bulk aerosol TI/TSI ratios from seven campaigns (colour coded); the black box indicates the latitudinal range of the campaigns at mid-latitudes reporting only TSI, and the red dashed line indicates the latitude of Neumayer II (S33). Panel b: Regression (considering error in both coordinates) of bulk aerosol TI vs TSI for all the available dataset and for a restricted dataset within the box indicated in panel a. Note that the fit is performed in the linear scale, although the scales are shown in the plot as logarithmic for better visualization of the lower values.

Figure 2 shows a strong linear correlation between bulk TI and TSI for seven campaigns where both quantities were measured (C5, C7, C11, C13, S14, S34, S35). We exclude C12 from this fit because

for three out of eight data pairs $TSI > TI$ beyond analytical uncertainty in TSI and TI, which suggests overestimated TSI in this campaign. The regression line (considering error in both coordinates) is given by:

$$TI/\text{pmol m}^{-3} = (1.6 \pm 0.4) + (1.34 \pm 0.06) \times TSI/\text{pmol m}^{-3} \quad (1)$$

The regression line is the same within error if the dataset is restricted to the zonal band where the TSI data needing scaling were acquired, but the p -value of the intercept increases from $p = 3 \times 10^{-4}$ for the full latitude range to $p = 0.02$, i.e. the intercept is not significantly different from zero at 99% confidence level. This is an indication of a number of measurements at high latitudes with a higher TI/TSI ratio, i.e. a higher NSI fraction, which can be readily seen in Figure 2. Thus, the TSI fraction appears to be quite stable ($\sim 75\%$), with excursions mainly concentrated at high latitudes. We use equation (1) to convert TSI measured in C4, C6, C8, C9, C10, C14, C17, C18, C19, S32, S33 and S36 into TI.

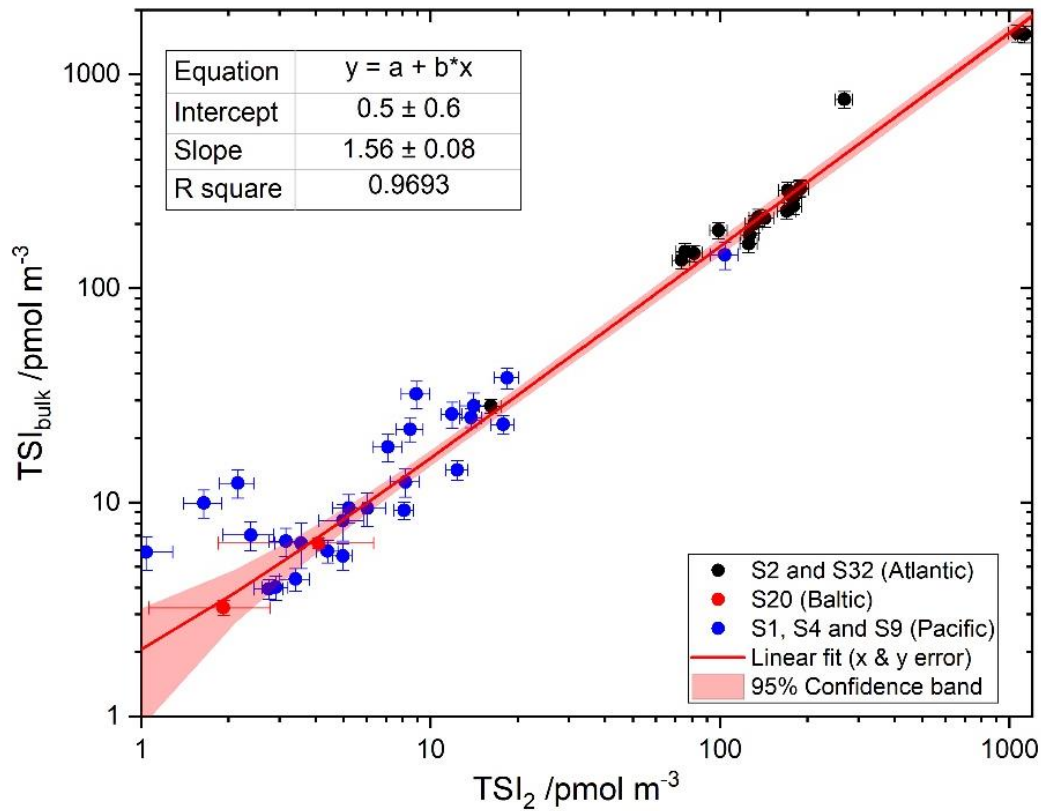


Figure 3. Regression of bulk TSI vs TSI for aerosol smaller than $\sim 2 \mu\text{m}$ (TSI_2). Black points: S2 (Cambridge, USA) and S32 (Mace Head, Ireland); red points: S20 (Finland); blue points: S1, S4 and S9 data from Pacific mid-latitudes). Note that the fit is performed in the linear scale, although the scales are shown in the plot as logarithmic for better visualization of the lower values.

It is also desirable to convert $PM_{2.5}$ TSI into bulk TSI in order to make the cruise campaigns C8 and C9 comparable to the rest. However, most campaigns reporting TSI in fine and coarse aerosol from cascade impactor measurements established the cut-off diameter at $1 \mu\text{m}$ (C4, C6, C10, C14, C17 and C19) instead of at $2.5 \mu\text{m}$, and do not report single stage data. Only S20 and S28 report coarse and fine data with $2.5 \mu\text{m}$ cut off. For S1, S2, S4, S9, S32, CI data segregated in narrow bins has been

reported, which can be aggregated for $d < 2\text{-}3\ \mu\text{m}$. S1, S2, S4 and S9 reported TI, but it can be transformed to TSI using equation (1). The S32 CI data for $d \leq 2\ \mu\text{m}$ shows a near to 1:1 relationship with concurrent S32 $\text{PM}_{2.5}$ measurements with $R^2=0.735$ ($p = 2 \times 10^{-5}$), indicating that CI data can be used to approximate $\text{PM}_{2.5}$ data. Figure 3 shows a regression of TSI data in bulk aerosol against TSI for $d < 2\text{-}3\ \mu\text{m}$ (termed TSI_2). It can be seen that the fraction of soluble iodine in aerosol with $d < 2\text{-}3\ \mu\text{m}$ appears to be fairly stable ($\sim 64\%$):

$$\text{TSI}_{\text{bulk}}/\text{pmol m}^{-3} = (0.5 \pm 0.6) + (1.56 \pm 0.08) \times \text{TSI}_2/\text{pmol m}^{-3} \quad (2)$$

The size segregated data from Alert (S28) is not considered in the fitting of Eq. (2), because most of the iodine mass observed in this campaign was in $\text{PM}_{2.5}$, which is an indication of a distinct partitioning in Polar regions. Equations (2) and (1) can now be used to transform the TSI $\text{PM}_{2.5}$ data of C8 and C9 into TI.

The PS14 TI datapoint in the Tropical Atlantic (C3) has been estimated here from the reported I^- and IO_3^- concentrations by obtaining first a TSI estimate using the average $\text{SOI}/\text{TII} = 0.42 \pm 0.22$ in the Tropical Atlantic (C4, C6 and C10, excluding observations close to the African coast for which SOI may be higher than in the open ocean), and then applying Eq. (1).

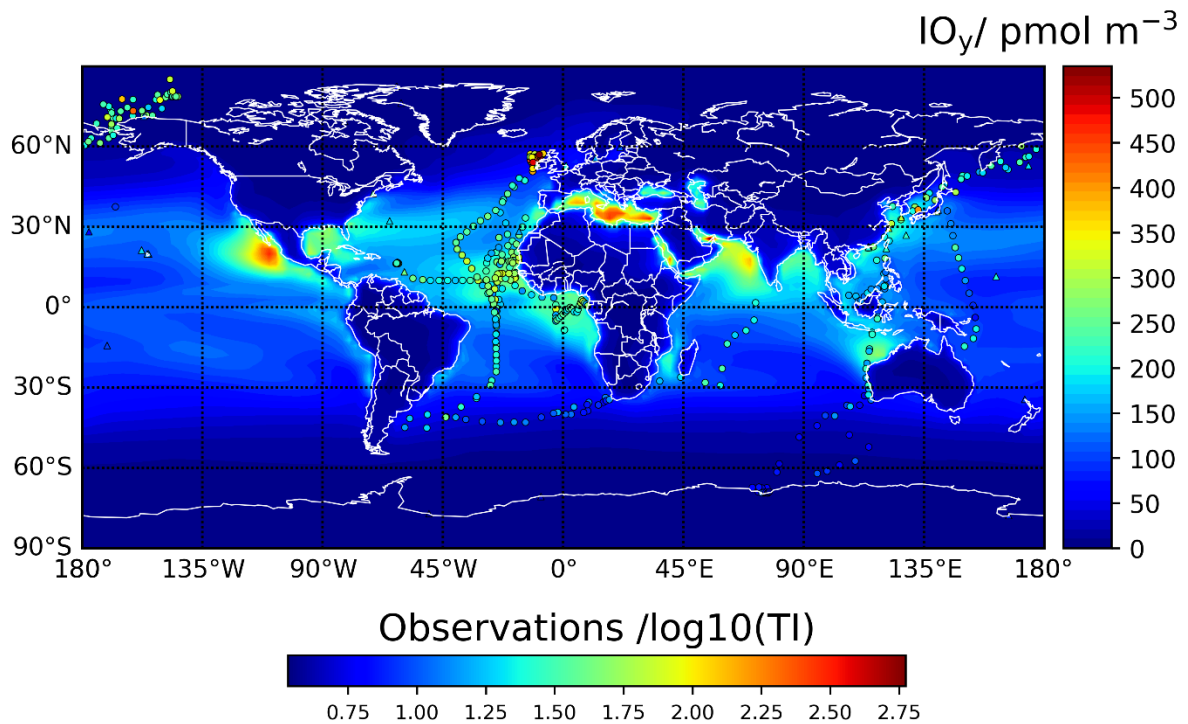


Figure 4. Global distribution of TI observations and TI estimates from TSI observations (plotted as $\log(\text{TI}/(\text{pmol m}^{-3}))$). The underlying colour map shows the average of modelled total inorganic gaseous iodine (IO_y) in the 1963-2010 period.

The full aerosol TI dataset is presented in Figure 4 using a logarithmic color scale, overlaid on a gas-phase IO_y global map. Figure 5a shows the data as a function of latitude. Figure 5b shows the ground-based campaign averages and the cruise data averaged in 10° intervals. The complete field dataset can

be found in a spreadsheet in the Supplementary Material of this paper.

Figure 4 shows that CAM-Chem predicts enhanced IO_y levels in tropical regions, specially towards the NH, as well as in the Mediterranean Sea. The TI and TSI field measurements sample well the Atlantic region, but campaigns in other areas with enhanced levels, such as the NH Eastern Pacific, the Gulf of Mexico, the Mediterranean Sea and the Arabian Sea, have not been carried out.

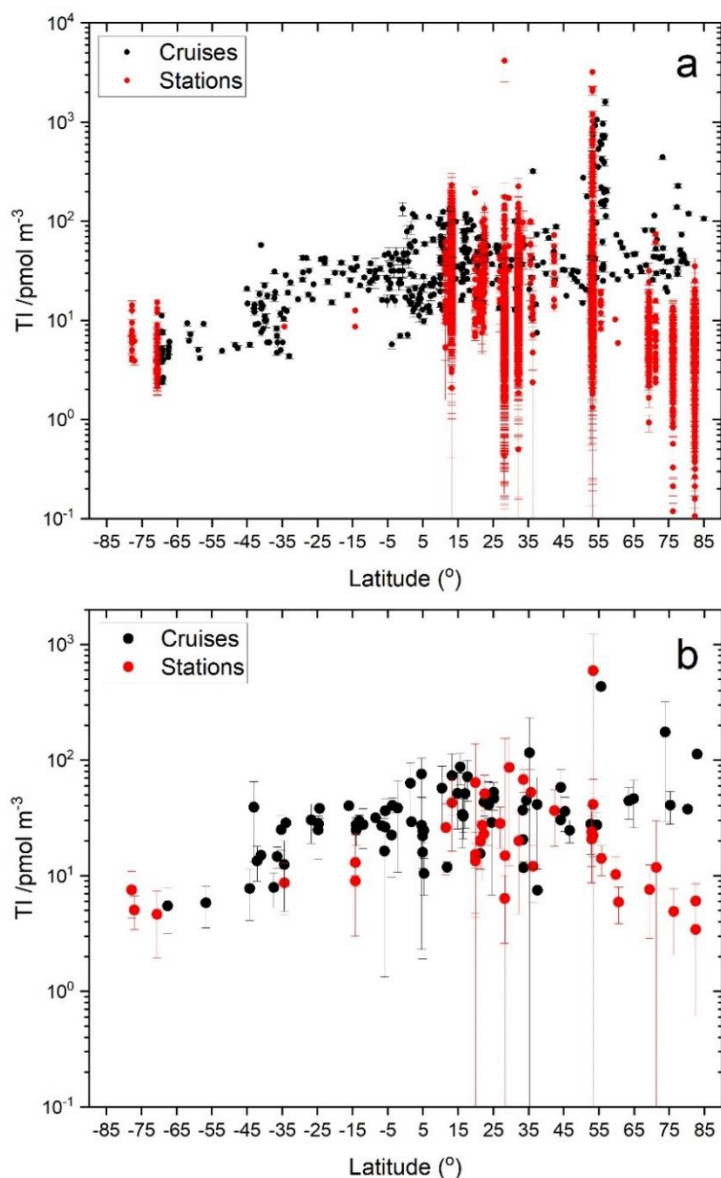


Figure 5. Latitudinal dependence of TI. Panel a: data points with error bars (for samples the error bars represent the analytical uncertainty, for full campaign averages the error bars are not shown). Panel b: campaign averages with error bars (standard deviation of each campaign). The data of each cruise is shown binned into 10° zonal band averages

3.2. Relationship between aerosol TI and gas-phase IO_y and TI_y

Gas-phase IO_y was measured alongside aerosol TI in the campaigns C1 (Equatorial Atlantic), S1 (Tropical North Pacific) and S29 (coastal Antarctica). TI_y was measured in the campaigns S5 (Tropical North Pacific) and S6 (coastal Antarctica), and can also be determined from the GOI

measurements performed in S29. Figure 6 shows that the average and range of the TI/IO_y and TI/TI_y ratios are very similar and do not show a dependence on geographical location beyond the range of variability. The proximity of the TI/IO_y and TI/TI_y ratios in the tropics and mid-latitudes can be expected, considering that the contribution of GOI to TI_y at those locations, as well as throughout the tropical free-troposphere, is expected to be $\sim 20\%$ [Saiz-Lopez *et al.*, 2014; Prados-Roman *et al.*, 2015a; Koenig *et al.*, 2020]. The relative invariance of the aerosol to gas phase ratio may be used to scale the TI_y or IO_y computed by CAM-Chem to make them comparable to the observations in absolute terms.

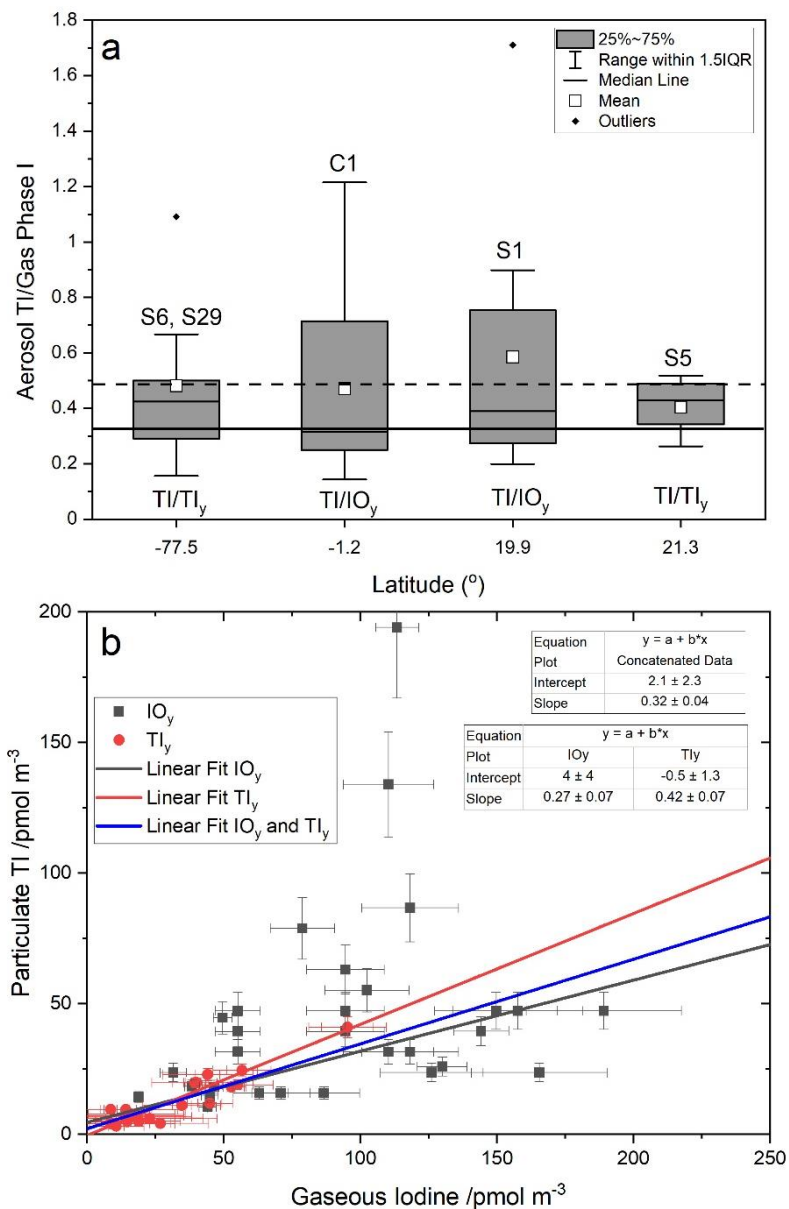


Figure 6. Panel a: box and whiskers plot showing statistics of TI/TI_y and TI/IO_y ratios at four latitudes (for the cruise C1 the average latitude is shown). IQR = interquartile range. The horizontal dashed line shows the unweighted average of the 56 ratios available. Panel b: Linear regressions with instrumental error in both coordinates of measured particulate TI vs measured gas-phase iodine (TI_y , IO_y and both). The horizontal solid line in Panel a corresponds to the slope of the concatenated fit (0.32), which is roughly the same as the error-weighted average of the 56 points.

Figure 6 indicates that the particulate TI vs gaseous iodine ratio takes values between ~0.3 (error-weighted average of the 56 datapoints, and also the fit with error in both coordinates in Figure 6b) and ~0.5 (the unweighted average in Figure 6a). Independent fits of the IO_y and TI_y scatterplots gives ratios of 0.27 and 0.42 (Figure 6b). Therefore, the gaseous iodine concentration is on average between 2 and 3 times higher than the iodine concentration in aerosol. A caveat to this result is that 54 out of the 56 datapoints in Figure 6b were measured between 1963 and 1979, which could affect the IO_y to TI conversion for more recent periods of time if the ratio has changed significantly since them.

3.3. Spatial and temporal variability of aerosol iodine

3.3.1. TI statistics by campaign

Table 4 lists descriptive statistics of the field campaigns described in Table 2 and Table 3. These statistics (arithmetic mean, standard deviation, geometric mean, geometric standard deviation, minimum, first quartile, median, third quartile and maximum) have been calculated from the individual sample data available. For those campaigns for which the data could not be retrieved, the statistics reported in the corresponding paper are included in the table (campaigns highlighted in bold font). In the particular case of S30, a monthly box and whisker plot with medians, quantiles, maximum and minimum is provided in the original publication, from which the maximum and minimum values of the full campaign are given in the table. The median of the campaign is calculated as the median of the monthly medians, and the arithmetic mean is estimated for plotting purposes as the average of the monthly maxima and minima (estimated values are given in italics).

Table 4. Statistics of total iodine (TI) in bulk aerosol (units: pmol m^{-3})^a

#	N	Mean	SD	Geo Mean	Geo SD	Min	Q1	Median	Q3	Max
C1	24	46.6	30.7	39.1	1.8	15.8	23.6	39.4	51.2	134.0
C2	17	7.5	7.2	7.5	2.3	--	--	--	--	--
C3	1	31.6	--	--	--	--	--	--	--	--
C4	28	43.0	32.1	33.5	2.0	12.8	18.6	26.6	61.8	124.3
C5	44	39.1	15.9	36.1	1.5	14.5	28.6	38.2	46.0	81.0
C6	22	34.7	15.3	32.2	1.5	15.0	24.7	32.0	38.2	81.5
C7	57	16.2	15.8	10.9	2.4	2.4	5.0	9.4	23.4	68.7
C8	33	432.8	358.4	296.1	2.6	33.1	157.5	352.6	693.9	1593.7
C9	14	13.8	4.0	13.2	1.3	7.6	11.6	13.2	16.8	22.3
C10	14	60.2	25.2	56.1	1.5	35.1	42.3	53.7	69.2	118.0
C11	17	48.5	21.4	44.0	1.6	16.0	33.1	47.6	57.3	97.1
C12	8	33.4	12.5	31.4	1.4	17.8	25.1	29.8	43.9	52.0
C13	28	88.3	95.9	61.3	2.2	20.0	30.5	53.5	103.0	443.0
C14	13	20.8	12.7	17.2	1.9	5.7	10.7	14.4	27.1	44.4
C15	11	7.9	2.6	7.5	1.4	5.0	6.0	7.0	10.0	13.0
C16	24	58.5	38.9	44.9	2.2	7.0	24.0	53.5	90.5	134.0
C17	33	43.7	21.8	39.5	1.6	18.2	29.7	41.4	48.7	111.0

C18	11	15.2	4.3	14.7	1.3	11.0	12.5	13.1	18.3	22.9
C19	10	29.0	8.5	28.0	1.3	18.1	23.1	27.0	35.0	42.6
S1a	5	63.8	73.8	42.1	2.6	14.9	25.9	39.5	44.6	194.1
S1b-d	4	15.3	3.7	14.9	1.3	10.4	12.3	16.2	18.2	18.3
S2	10	36.5	18.6	32.3	1.7	13.8	23.2	34.7	45.7	72.5
S3	23	11.8	18.1	7.0	2.4	2.4	3.7	6.7	10.2	74.1
S4	8	13.4	9.0	11.4	1.8	6.9	7.2	9.3	17.2	32.6
S5	11	19.7	8.3	18.4	1.5	11.0	12.6	18.9	22.9	41.0
S6	19	7.5	3.3	7.0	1.5	4.0	5.0	6.7	9.5	14.2
S7	287	14.2	9.5	--	--	--	--	--	--	--
S8 ^b	135	4.9	2.9	3.9	2.3	0.1	2.8	4.6	6.3	13.6
S9	27	26.0	15.8	21.1	2.0	5.3	12.6	22.9	37.0	62.3
S10 ^c	110	7.6	4.7	6.4	1.8	0.9	4.1	6.5	10.0	31.5
S11	1234	3.4	2.8	2.6	2.2	0.1	1.6	2.8	4.5	35.1
S12a	7	<i>13.0</i>	<i>10.0</i>	12.6	2.0	--	--	--	--	--
S12b	4	<i>9.0</i>	<i>1.0</i>	8.7	1.1	--	--	--	--	--
S13	11	8.7	4.1	--	--	--	--	--	--	--
S14	9	52.4	30.1	44.4	1.9	13.4	36.2	44.9	59.1	100.1
S15	1308	20.0	15.3	16.4	1.9	0.5	10.8	16.3	24.2	224.6
S16	2750	42.7	26.5	36.1	1.8	2.1	24.6	36.5	54.0	231.7
S17	905	14.9	138.7	7.3	2.2	1.5	4.4	6.4	11.0	4160.8
S18	436	22.3	29.2	14.9	2.4	1.3	8.4	14.0	26.2	424.0
S19	13	12.1	6.2	10.4	1.9	2.4	10.2	11.0	15.0	26.8
S20a	35	10.2	4.2	--	--	--	--	--	--	--
S20b	35	5.9	2.1	--	--	--	--	--	--	--
S21	12	6.4	3.7	4.9	2.5	0.4	3.6	6.0	8.6	13.8
S22	50	51.2	22.8	46.9	1.5	19.1	35.9	42.9	63.4	134.0
S23	29	27.3	18.3	22.8	1.8	7.5	13.9	23.8	37.8	97.7
S24	8	28.2	11.0	26.3	1.5	15.0	18.6	28.0	36.3	44.8
S25	6	67.9	15.3	66.7	1.2	54.2	61.1	63.2	67.9	97.7
S26	37	20.3	8.9	18.9	1.4	9.6	15.2	19.1	22.9	56.1
S27	15	20.7	12.0	18.0	1.7	6.5	13.2	18.0	25.1	55.0
S28	85	6.0	2.5	5.6	1.5	2.1	4.0	6.0	7.5	16.3
S29	2	5.0	1.6	--	--	3.9	--	--	--	6.2
S30	114	<i>23.0</i>	<i>14.0</i>	--	--	1.8	--	21.9	--	91.3
S31	16	24.1	12.0	20.8	1.8	5.4	13.7	23.9	32.0	50.5
S32	45	593.5	629.5	424.4	2.14	69.79	260.8	352.95	634.0	3208.6
S33	56	4.6	2.7	4.1	1.6	2.1	2.8	3.6	5.3	15.2
S34	3	41.3	26.7	33.8	2.3	13.0	13.0	45.0	66.0	66.0
S35	8	14.1	4.1	13.5	1.4	8.2	10.6	14.7	17.3	19.5
S36	3	86.3	74.2	67.5	2.3	32.2	32.2	55.9	170.8	170.8

^a Campaigns for which only statistics have been published and for which the original data could not be retrieved are highlighted in bold font. For the rest of the campaigns the statistics have been calculated from the available datapoints. SD, Geo Mean, Geo SD, Min, Q1, Q3 and Max are respectively the standard deviation, the geometric mean, the geometric standard deviation, the minimum, the first quartile, the third quartile and the maximum. Values in italics: the arithmetic mean and standard deviation have been estimated for plotting

purposes, because the original papers only report the geometric mean and geometric standard deviation. ^b Mould Bay: The arithmetic mean and standard deviation of a subset of 67 measurements reported in the original paper are (4.0 ± 3.2) pmol m⁻³. TI statistics for the full dataset were not reported [Sturges and Barrie, 1988]. ^c Igloolik: The arithmetic mean and standard deviation of a subset of 67 measurements reported in the original paper are (8.1 ± 5.1) pmol m⁻³. TI statistics for the full dataset were not reported [Sturges and Barrie, 1988].

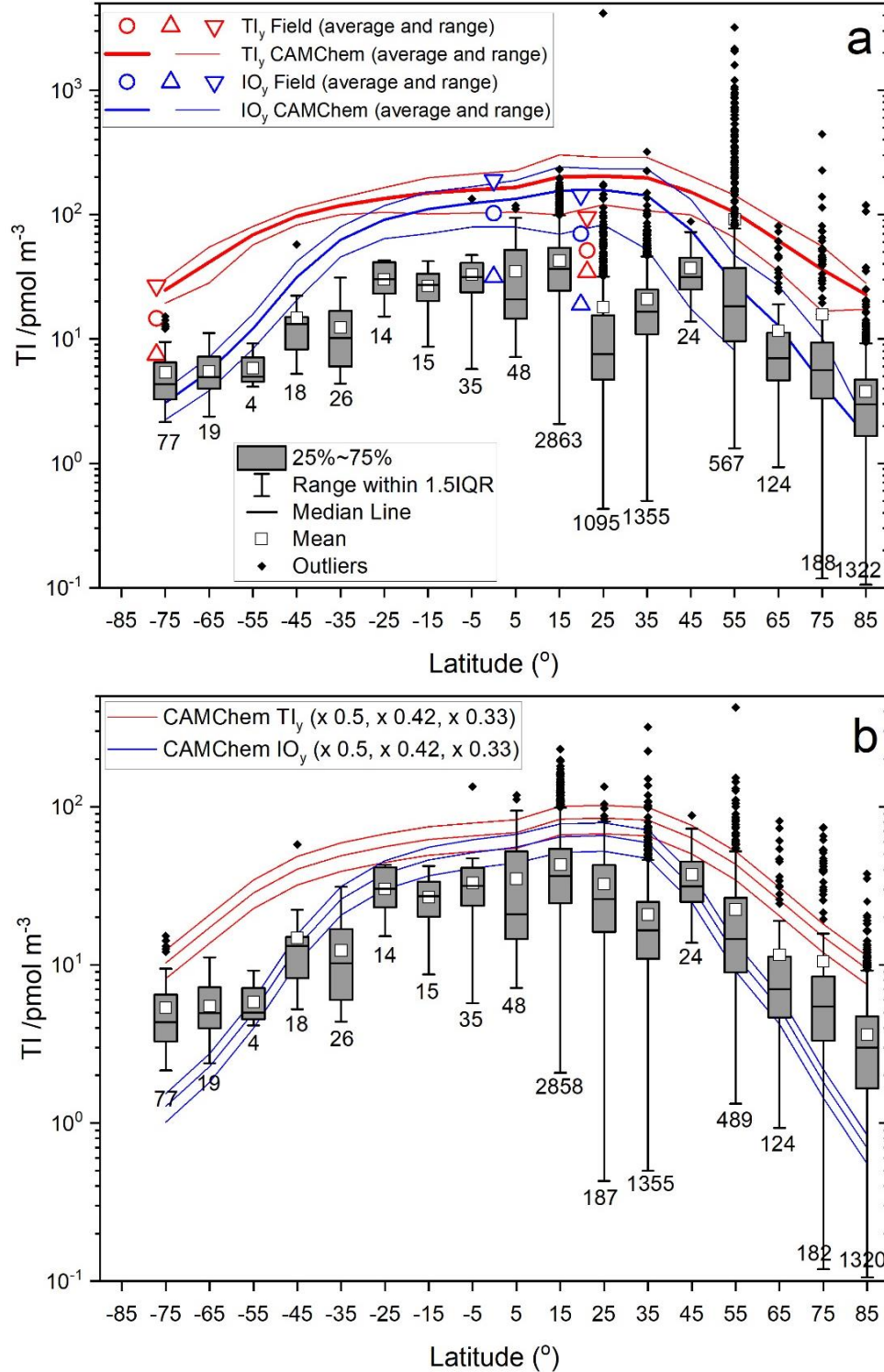


Figure 7. Latitudinal dependence of bulk aerosol total iodine. The box and whiskers statistics of available datapoints correspond to 10° zonal bands. The numbers below each whisker indicate the datapoints within each zonal band. Panel a: TI statistics of all campaigns listed in Tables 1 and 2. Circles and triangles indicate the average, maximum and minimum IO_y (blue symbols) and TI_y (red symbols) measured in 5 campaigns. Solid blue and red lines indicate the 1950-2010 average and ranges of IO_y and TI_y, respectively, computed with CAM-

Chem. Panel b: as panel a, but excluding high altitude data (Izaña and Mauna Loa observatories), data potentially affected by new particle formation (North Atlantic and Mace Head MAP 2006 measurements, Chinese coast measurements) and Arctic cruises potentially affected by sea ice loss (samples of the 3rd China Arctic Research Expedition collected in the Arctic Ocean). Panel b also includes the simulated 1950-2010 averages of IO_y and TI_y scaled by factors 0.5, 0.42 and 0.33, as indicated by the analysis in Figure 6. Note the different vertical scale in the two panels.

3.3.2. Latitudinal dependence

Figure 5a with all the datapoints and Figure 5b with the campaign averages show a clear dependence of TI on latitude. To highlight these features, Figure 7a shows the complete bulk aerosol TI dataset plotted vs. 10° wide latitudinal bands in box and whisker fashion. All statistics show a clear latitudinal dependence, with TI peaking in the tropical regions and decreasing towards the poles, although there is a hemispheric asymmetry where the values in the northern hemisphere (NH) tend to be higher than in the southern hemisphere (SH). As a note of caution, there is a heavy hemispheric sampling imbalance, with the majority of the samples taken in the NH ($n = 208$ in the SH vs $n = 7586$ in the NH). There are many more outliers in the northern hemisphere, most of which result from the recent measurements in Mace Head (S32) and the Northern Atlantic (C8), as well as from observations in the Arctic Ocean (C13). The inclusion of high-altitude stations (S1b-d, S17), data possibly affected by new particle formation (C8 and S32) and data potentially affected by recent loss of sea ice (C13) may distort the long-term latitudinal dependence of aerosol TI.

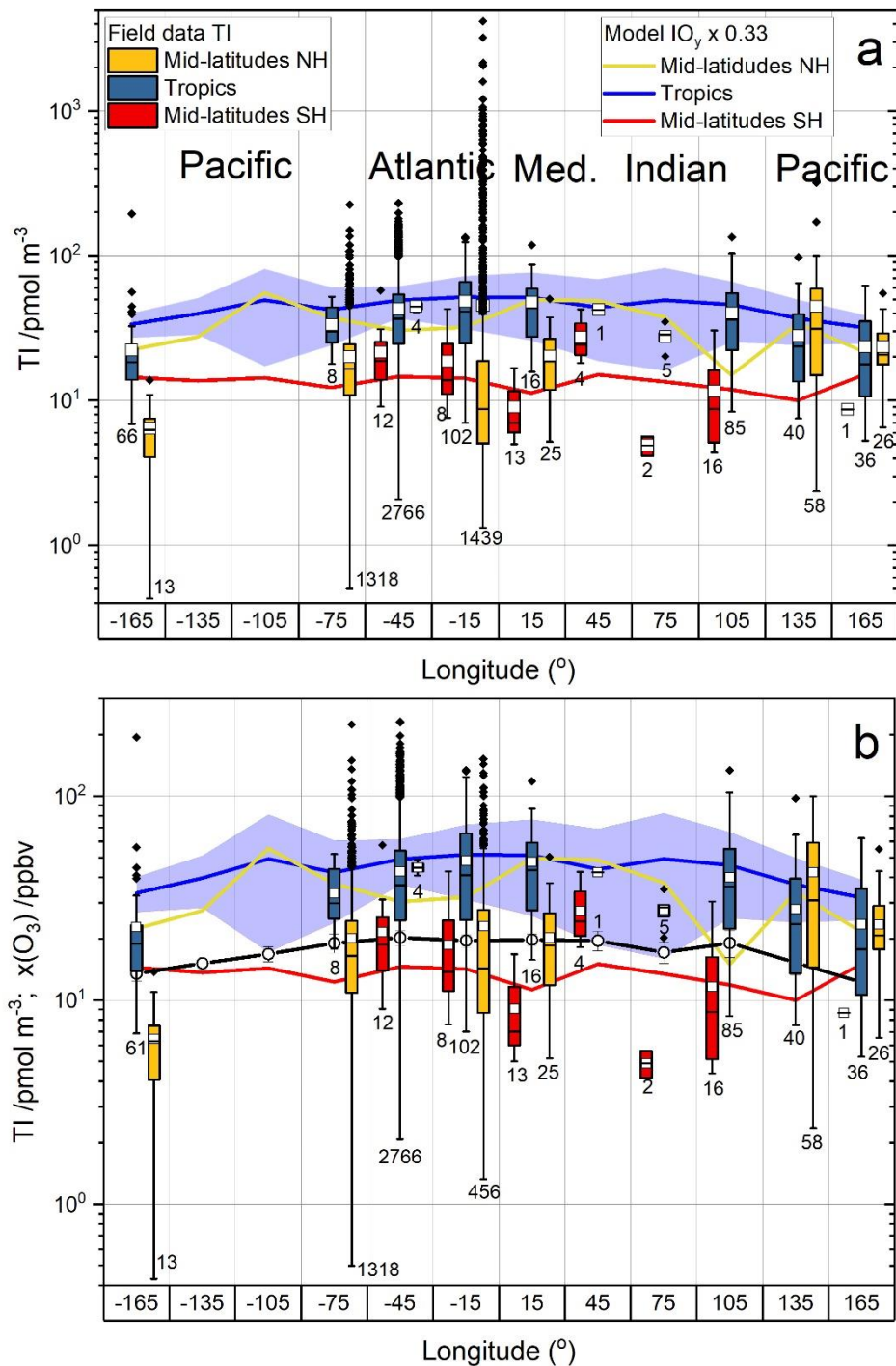
Figure 7b shows the latitudinal dependence of the TI data without the C8, S32, S1b-d, S16 and the Arctic transect of C13. This increases the average at 25° (by removing the high altitude low values at Izaña) and decreases the average at 55° and 75° (by removing high values in the northern Atlantic and the Arctic). Thus, besides the known lower values at high altitude, note that some recent NH TI data appears to be enhanced with respect to the historic record (see below).

A caveat to the analysis performed in Figure 7 is that for those zonal bands where most of the data corresponds to one or two stations (15°, 25°, 35°, 55°, 85°), the corresponding zonal average is totally dominated by these stations (Figure 5a). An alternative way of analyzing this data is grouping the campaign averages (Figure 5b) in zonal bands (Figure S1). By comparing Figures 7 and S1, it can be seen that the latitudinal dependence of sample and campaign zonal averages of TI is very similar, supporting the statistical analysis performed here.

3.3.3. Longitudinal dependence

Figures 8 and S2 show the longitudinal dependence of TI in bulk aerosol for datapoints and campaign averages, respectively. Within the tropics, the highest concentrations are observed in the Atlantic. At mid-latitudes in the NH, the data acquired during the 2006 MAP campaign at Mace Head (C8 and S32) enhances the average at -15° longitude (Atlantic). After screening the C8 and S32 data, likely affected by coastal and open ocean new-particle formation [O'Dowd *et al.*, 2002; O'Dowd *et al.*, 2010], it appears that the highest average concentration in the NH mid-latitudes occurs in South-East Asia (135° longitude). In the SH, the TI concentrations are somewhat lower in the Indian Ocean

468 compared to those in the Atlantic Ocean.



469 **Figure 8.** Longitudinal dependence of bulk aerosol total iodine. The box and whiskers statistics of available
 470 datapoints correspond to 30° meridional bands. The numbers of datapoints within each meridional band
 471 appears under the corresponding box. Box and whiskers statistics as in previous figures. The red and yellow
 472 boxes correspond to respectively to SH mid-latitudes (60°S to 25°S) and NH mid-latitudes (25°N to 60°N), and
 473 the blue boxes to low latitudes (25°S to 25°N). Panel a: all mid- and low latitude campaigns listed in Tables 1
 474 and 2. Panel b: as panel a but excluding high altitude data (Izaña and Mauna Loa observatories) and data
 475 potentially affected by new particle formation (North Atlantic and Mace Head MAP 2006 measurements). Both
 476 panels show the IO_y 1950-2010 average computed by the model for the corresponding latitudinal band, scaled
 477 by a factor of 0.33. The blue shaded region indicates the span of the IO_y range (1950-2010) in the tropics. The
 478

bottom panel also shows the surface O_3 1950-2010 average computed by the model in the tropics (thick black line and empty circles). Note the different vertical scale in the two panels.

3.3.4. Seasonal variation

Figure S3 shows the monthly climatology of total iodine in bulk aerosol for six different latitudinal bands. For mid-latitudes and tropics, the climatologies are also divided into Atlantic and Pacific. The seasonal variability in the Arctic and in Antarctica are similar, presenting equinoctial maxima, with the spring maximum showing enhanced values. At Atlantic and Pacific NH mid-latitudes, aerosol iodine does not show a discernible seasonal variation, but there are hints of seasonal cycles in the NH tropics. The TI data for SH low and mid-latitudes is too sparse to draw any conclusions. It must be pointed out, nevertheless, that only a few campaigns at specific sites report year-long measurements, which can yield a proper climatology. Thus, averaging of dissimilar datasets with sparse monthly coverage in different years and at widespread locations may result in unrealistic TI climatologies. This is especially true considering that local weather seasonal cycles as well as local iodine sources may vary significantly within the same zonal and meridional band. For example, the Antarctic seasonal variation was recorded almost entirely in Neumayer II between January 2007 and January 2008, while only a few measurements in spring and summer were carried out at Filchner station (S29) and McMurdo (S6). Thus, the “Antarctic” TI seasonal cycle plotted in Figure S3 is mainly the cycle at Neumayer II, which may not be representative of the entire Antarctic coast. This is also the case for other regions: the climatology in the NH tropical Atlantic is dominated by the multi-year AEROCE measurements at Barbados (S16), while the year-long dataset recorded at Hong-Kong (S30) determines the monthly statistics in the tropical Pacific. Additional data from other campaigns with incomplete coverage only distort the local cycles without bringing in additional information. For this reason, we plot in Figure 9 the monthly climatologies for each of the nine stations where year-long measurements of TI or TSI have been carried out (S8, S10, S11, S15, S16, S18, S19, S30, S33). Seasonal cycles can be observed at Mould Bay (S8), Alert (S11) and Neumayer II (S33), with a similar double peak profile as mentioned above. The lack of a clear seasonal variation at Igloolik compared to Mould Bay and Alert was already noticed by Sturges and Barrie [1988]. Measurements at mid-latitude stations (S15, S18 and S19) do not show a clear seasonal variation. Note that the data acquired during the MAP campaign in June-July 2006 at Mace Head (S32) is anomalously high compared to the June and July averages of the AEROCE campaign between 1989 and 1994 (S18). In the NH tropics, Barbados (S16) and Hong-Kong (S30) show cycles which are mutually out of phase (the July maximum of S16 coincides with a minimum of S30). Although S30 was a one-year campaign, the high frequency measurements during S22 (September-November) appear to confirm an annual cycle peaking toward the end of the year.

3.3.5. Long-term trends

Box and whiskers plots of total iodine measurements grouped by year are shown in Figure 10. The

long-term series in Figure 10 suggest that increases in TI may have occurred between 1963 and 2010. However, both linear and exponential (i.e. apparent linear fitting of the semi-logarithmic scatter plot) unweighted fits of the annual averages indicate that the only slope significantly different from zero at 95% confidence level occurs in the Tropics ($4.4 \pm 1.6 \text{ pmol m}^{-3} \text{ decade}^{-1}$, $p = 0.013$), resulting in a factor of ~ 2 increase between 1963 and 2010. The NH data at middle and high latitudes is compatible both with decreasing and increasing trends (confidence bands in Figure 10). Even though the evolution of TI abundances between 1963 and 2010 show a more pronounced trend moving from the NH high-latitudes to the tropical regions, this should be taken with caution, as only a few observations have been performed within the exact same location to enable any conclusion regarding the latitudinal variation of the TI long-term evolution.

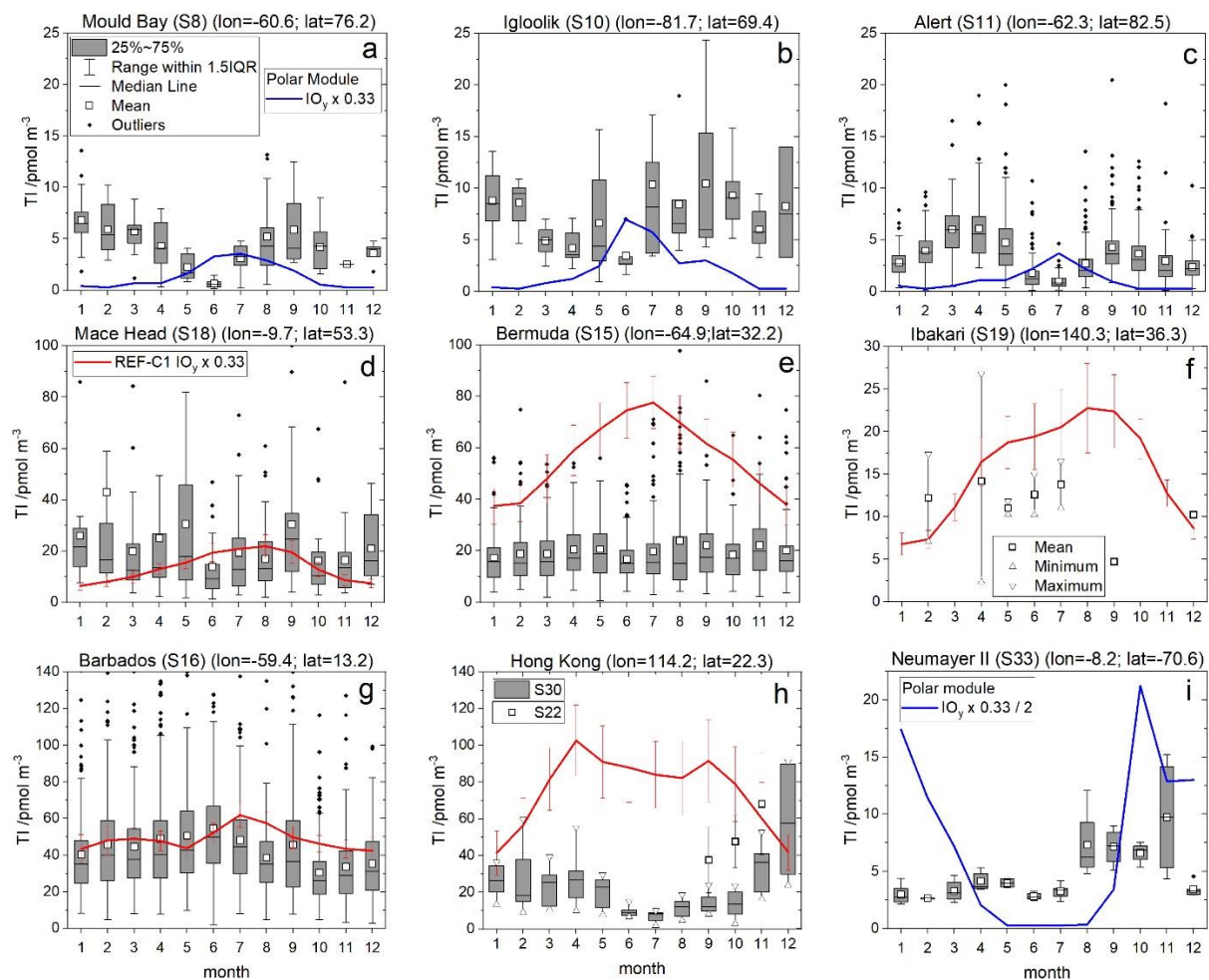


Figure 9. Bulk aerosol TI climatologies in nine stations. The box and whiskers statistics are defined as in previous figures. In panel f, monthly averages, maxima and minima of a limited dataset acquired at Ibakari (S19) are shown. In panel h the box and whiskers plot for S30 shown in the corresponding reference is reproduced (no mean reported, only median values), with the triangles indicating maxima and minima. Panel h also incorporates PEM WEST A measurements at Hong-Kong (S22) with a high sampling frequency but just for three months. The solid red lines correspond to the REF-C1 climatologies of scaled IO_y for the 1950-2010 period (error bars indicate variability within that period), while the polar module IO_y climatology for year 2000 is shown in blue. A scaling factor of $TI/IO_y = 0.33$ is used in all cases.

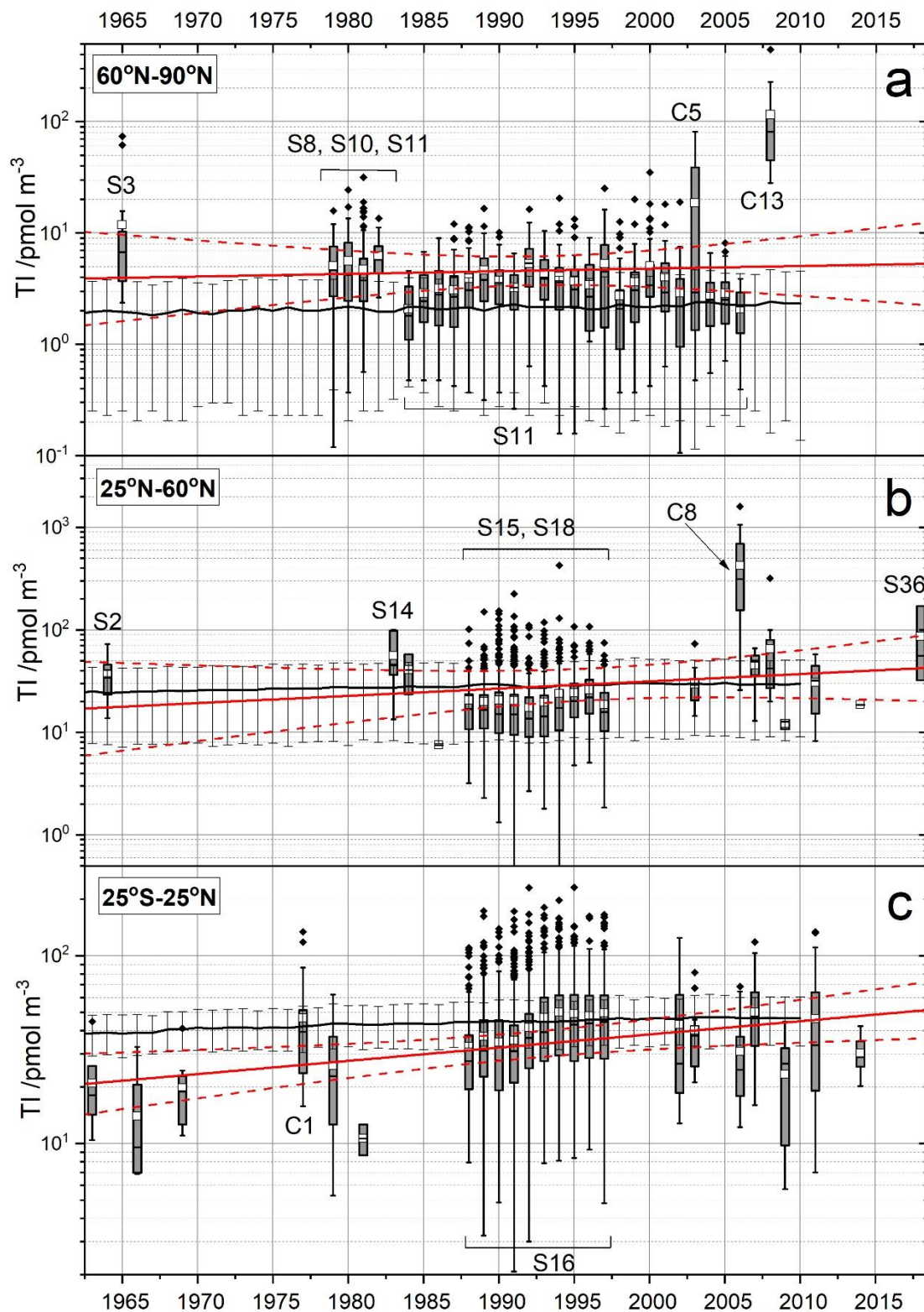


Figure 10. Long-term variation of the annual averages of TI in bulk aerosol for three zonal bands: Arctic (panel a), NH mid-latitudes (panel b) and tropics (panel c). Measurements at mid- and high SH locations are sparse and therefore these latitudinal bands are omitted. High altitude data (Izaña, Mauna Loa) and data clearly affected by coastal particle formation (Mace Head, S32) have been omitted from the statistics calculations. The box and whiskers statistics are defined as in previous figures. Data belonging to key campaigns are identified in the plot. The trend lines (red) represent unweighted apparent (exponential) fits of all the annual averages shown (dashed lines represent the 95% confidence bands of the fits). The annual averages of modelled IO_y in the corresponding zonal bands are shown by black lines.

4. Discussion

4.1. Latitudinal dependence

The latitudinal profile of aerosol TI is reminiscent of the sea water I⁻ profile [MacDonald *et al.*, 2014; Prados-Roman *et al.*, 2015a; Chance *et al.*, 2019]. Thus, aerosol iodine likely tracks the emission fluxes of the dominant iodine source, which is the I⁻ + O₃ reaction in the ocean surface [Carpenter *et al.*, 2013]. The hemispheric asymmetry results from the higher abundance of O₃ in the NH as a result of anthropogenic pollution [Prados-Roman *et al.*, 2015a; Cuevas *et al.*, 2018].

The ratio TI/TSI is key to homogenize the most recent cruise data and make it directly comparable to the TI measurements. Although speciation will be discussed in a follow up work, it is worth mentioning here that the TSI group dominates TI almost everywhere except in the high latitudes, where there is some evidence of enhanced NSI (Figure 2). In the particular case of the new dataset from Neumayer II (S33), TSI values are low and comparable to the intercept of equation (1). Thus, the TI values obtained with equation (1) for S33 result in a relatively high TI/TSI ratio (S33 average of 2.6 ± 0.9). This is consistent with the higher values of TI/TSI at high latitudes shown in Figure 2a (TI/TSI = 2.4 ± 2.3 at high latitudes, TI/TSI = 1.6 ± 0.7 at middle and low latitudes inside the black box in Figure 2a), but it must be kept in mind that TI/TSI values closer to 1 are also registered in a full campaign at high latitudes (C13), and therefore equation (1) may overestimate TI at Neumayer.

Model TI_y and IO_y are comparable to the average TI after scaling by a factor of 0.3-0.5, which is obtained from campaign where both gas-phase and aerosol iodine were measured. The agreement between the REF-C1 simulated TI_y and IO_y scaled averages is good at low and mid-latitudes, where TI_y ~ IO_y. At high latitudes, a larger fraction of TI_y is in the form of GOI, which explains why scaled TI_y overestimates TI. By contrast, scaled IO_y underestimates TI. Since the polar module was not run in the REF-C1 simulation, ice sources of inorganic iodine are not accounted for, and therefore the model produces less IO_y [Fernandez *et al.*, 2019], which explains why the scaled IO_y curves lie below the TI observations.

4.2. Longitudinal dependence

In the tropics, TI is enhanced in the Atlantic, which results from a combination of high biogenic activity in the equatorial Atlantic (especially close to the Gulf of Guinea, as shown by the R/V Capricorne observations) and the zonal wave-one pattern of tropical tropospheric O₃ [Thompson *et al.*, 2003], which peaks in the Atlantic and enhances the inorganic source. A caveat is the lack of measurements in the tropical eastern Pacific. The modelled IO_y has a similar longitudinal dependence than the TI statistics, although smoother and with a less pronounced Pacific minimum (Figure 8). CAM-Chem reproduces correctly the wave-one longitudinal dependence of tropospheric and surface O₃ in the tropics (Figure 8b), which indicates that the longitudinal dependence of airborne iodine is in fact controlled by ozone through the ocean surface inorganic source.

TI shows a relative maximum in the NH Western Pacific, most likely as a result of O₃ pollution

outflowing from China, perhaps with an additional contribution of biogenic iodine source gases resulting from extensive algae farming. CAM-Chem also predicts a local maximum of TI_y (Figure 4) and IO_y (Figure 8), as well as of O_3 [Prados-Roman *et al.*, 2015a] at those latitudes. The high average IO_y values predicted by the model at mid-latitudes in the NH for the 15° and 45° meridional bands shown in Figure 8 result from the high concentrations above the Mediterranean Sea (Figure 4). Although the concentration of I^- in Mediterranean seawater is not particularly high [Chance *et al.*, 2019], the Mediterranean basin shows elevated ozone concentrations, which are expected to significantly enhance I_2 and HOI emissions [Prados-Roman *et al.*, 2015a]. The three campaigns in the 15° meridional band at mid-latitudes took place at the top latitude end (Scandinavia) and show lower TI concentrations than the average model prediction, although in agreement with the model predictions for those locations (Figure 4).

Sherwen *et al.* [2016a] implemented in GEOS-Chem the same on-line oceanic iodine source developed for CAM-Chem and compared their modeling results with a subset of cruise TSI measurements. Their global maps of modelled TI suggest latitudinal and longitudinal variations that are consistent with the spatial variations demonstrated by the TI field data compiled in this work. The average TI absolute values modelled by GEOS-Chem are consistent with the TI field observations and the agreement with the subset of TSI measurements considered by Sherwen *et al.* improves if equation (1) is used to convert observed TSI into TI.

4.3 Seasonal variation

The seasonal profiles of TI in the Arctic (Mould Bay and Alert) and in Antarctica (Neumayer II) are similar, showing equinoctial maxima with an absolute maximum in the polar spring (Figure 9). The seasonal variation at Igloolik is less clear. While the TI seasonal profiles in the Arctic have been discussed previously, the TI Antarctic profile is reported in this work for the first time. This double seasonal peak is also observed in year-long IO measurements at Halley (Antarctica) [Saiz-Lopez *et al.*, 2007], and is well captured by the CAM-Chem polar module [Fernandez *et al.*, 2019]. We note that the long-term MAX-DOAS observations of IO at Neumayer reported by [Frieß *et al.*, 2010] do not show a detectable seasonality, although this was most likely due to observation conditions inherent to this technique and to sparse coverage during spring and autumn.

The seasonal dependence of airborne iodine in the polar regions of both hemispheres is determined by the interplay between radiation and sea ice-related sources [Fernandez *et al.*, 2019]. The primary spring maximum peak in both hemispheres is caused by enhanced photochemical reactions at polar sunrise. The seasonal variation of TSI in snow observed at Neumayer [Frieß *et al.*, 2010] and in the coastal East Antarctica Law Dome ice core [Spolaor *et al.*, 2014] shows a winter maximum and a sharp decrease in spring which result from volatilization of iodine from the snowpack. The spring maximum also coincides with phytoplankton blooms within the Weddell Sea. The secondary maximum in the SH is likely related to an enhancement of the surface sea ice flux resulting from the

rapid increase in first year sea ice during March and April before the austral polar sunset, combined with an increase of sea-salt aerosol dehalogenation. These processes are included in the polar module, which reproduces qualitatively the double-peaked seasonal cycle of TI at Neumayer II, while the scaled IO_y overestimates the TI values by a factor of 2 (Figure 9i), possibly as a result of the aforementioned lack of the IOP sink in the model. Note that the zonal average in Figure S3, panel f, overestimates the absolute values by a factor of 10, which results from the very high IO_y values predicted over the Weddell and Ross sea ice shelves as a result of seasonally dependent iodine ice sources.

In the Arctic, the polar module does not generate a double peak seasonal variation of IO_y , owing to the single seasonal maximum predicted for meridional iodine sources [Fernandez *et al.*, 2019]. This is at odds with the marked double peak seasonality of TI at Mould Bay (Figure 9a) and Alert (Figure 9c) and indicates that the iodine sources in the Arctic are not well understood. In fact, the polar module of CAM-Chem in the Arctic has not been yet fully tested owing to the scarcity of gas-phase iodine measurements in the region [Saiz-Lopez *et al.*, 2012a]. It has been proposed that the secondary NH maximum may be associated with a secondary bloom in marine biota and transport [Barrie and Barrie, 1990; Sharma *et al.*, 2019]. The lack of a clear seasonal cycle at Igloolik, which is free of ice for much of the year, has been previously attributed to a greater marine influence compared to Alert and Mould Bay. Note that a larger local marine source may mask the ice-related seasonal cycle [Sturges and Barrie, 1988].

The seasonal profiles at NH mid-latitudes in the Atlantic are rather flat (Figure 9, panels d and e), while the model predicts a summer IO_y maximum, coinciding with an O_3 minimum. CAM-Chem has been shown to reproduce the seasonality of surface ozone globally [Saiz-Lopez *et al.*, 2012b; Tilmes *et al.*, 2016]. This indicates that the seasonal behavior of airborne iodine is not only dependent on the seasonal variation of the iodine oceanic source, but also on other factors such as solar radiation, which may also decouple the seasonal variation of TI and IO_y . The scaled modelled IO_y overestimates the observations at Bermuda by a factor of 2 to 4, which is likely a consequence of the hotspot of sea-salt aerosol recycling predicted by the model in the North Atlantic [Prados-Roman *et al.*, 2015b], implying larger concentrations of gas-phase IO_y and a lower modelled TI/ IO_y ratio in this region than observed further south (Figure 6). Note that simultaneous measurements of TI (or TSI) and IO_y (or TI_y) in the North Atlantic have not been reported. In Mace Head the measured TI, which does not show a defined seasonal pattern, is likely influenced by frequent iodide-driven new particle formation events at the Irish coast [O'Dowd *et al.*, 2002]. The only long-term data in the Pacific (Ibakari, Japan, Figure 9f) are too sparse to draw any conclusions about seasonal cycles, although the model prediction is mostly consistent with the available data.

In the NH tropics (Barbados, Figure 9g), there is a late spring maximum and an autumn minimum in TI, which is broadly consistent with the weak seasonal cycle of modelled IO_y . In the tropical NH

western Pacific there is a deep minimum between July and October (Hong-Kong, Figure 9h), which is likely related to the specific wind patterns controlling the origin of aerosol in this region and not to the seasonal dependence of the iodine oceanic sources, since the concentrations of anthropogenic substances and mineral dust measured at Hong-Kong show a very similar seasonal dependence to TI [Cheng *et al.*, 2000]. In winter, the prevailing wind direction is from the north and north-east, which implies polluted air masses from China passing over sections of the coast. The modelled and scaled IO_y within the model pixel containing Hong-Kong Island overestimates the average TI values observed during the S30, but the agreement is better with the average values reported for the S22 campaign. A proper comparison of modelled and observed seasonal variations requires several years of observations and higher spatial resolution in the model.

4.4 Long-term trends

Figure 10 shows that the data in the tropics (3166 points) are more regularly spaced in time and that the range of TI values is narrower than at NH mid-latitudes (1979 datapoints) and NH high latitudes (1634 points). Some short-term campaigns carried out at middle and high latitudes show very high values (e.g. C5, C8 and C13) and point to iodine sources which may be active in specific time periods and locations (e.g. ocean surface and sub-ice phytoplankton blooms and sea ice loss and growth). Alert (S11) is at a higher latitude than Barrow (S3), Igloolik (S10), Mould Bay (S8) and most of the sampling points of the 2nd and 3rd CHINARE expeditions (C5 and C13). At Alert, the sea is covered with ice for most of the year (the ice pack does move out in the summer months, leaving open water). Barrow, Mould Bay, Igloolik and the Arctic sea locations of the CHINARE expeditions are more exposed to open water and have varying sea ice cover. If we ignore the Alert data in Figure 10a, there appears to be an increase in TI, which would be consistent with a doubling of the iodine concentration in sea ice between 1950 and 2010 recently reported [Cuevas *et al.*, 2018], possibly linked to enhanced phytoplankton production caused by the recent thinning of sea ice in the Arctic, combined with an enhancement of the ocean surface inorganic source. At NH mid-latitudes, the Cambridge (S2) and Tokyo (S14) campaigns are two decades apart, spatially widely separated, and they consist only of a handful of points. Ignoring those two stations and the anomalous S32 campaign at Mace Head, the data is consistent with an increase in TI from the beginning of the AEROCE campaign by a factor of 2-3.

The CAM-Chem REF-C1 run shows modest increases in IO_y between 1963 and 2010: 15%, 20% and 21% for NH high latitudes, NH mid-latitudes and the Tropics, respectively. It is worth emphasizing again that ice iodine sources are not included in REF-C1, and therefore the modeling predictions in the polar regions are missing the major contributions to the iodine burden in the polar regions, which are likely to be changing with time as a result of global warming. According to the GEOS-Chem results [Sherwen *et al.*, 2016a], global pre-industrial TI was 23% lower compared to present day, which is roughly consistent with the IO_y variation obtained from the CAM-Chem REF-C1 simulation.

5. Conclusions

The dataset of aerosol iodine measurements compiled in this work provides the first global-scale piece of empirical evidence about the major source of atmospheric iodine, i.e. the reaction on the ocean surface between aqueous I⁻ and deposited gas-phase O₃. Analysis of the field data shows that there are close to linear relationships between soluble and total iodine in aerosol (~75% aerosol iodine is soluble), and between soluble iodine in the bulk and the fine fraction (~64% aerosol iodine is in the PM_{2.5} fraction). These relationships enable converting soluble iodine and fine fraction iodine datasets into total iodine in bulk aerosol. Furthermore, the gaseous iodine concentration measured in several campaigns is found to be on average between a factor of 2 and 3 times higher than the total iodine concentration in bulk aerosol.

The latitudinal and longitudinal dependences of aerosol iodine track well the dependences of this source on temperature and ozone concentration, as shown by comparing the field data with model simulations where the parameterized oceanic iodine source is implemented. The seasonal variations at different zonal and meridional bands are less clear but appear to be directly influenced by regional weather climatology rather than by the seasonal variation of ozone. Long-term trends are difficult to establish due to the lack of homogeneity of the data, but nevertheless a significant positive trend is observed in the Tropics, which is consistent with model predictions about the enhancement of the oceanic iodine source as a result of increased anthropogenic ozone.

Acknowledgements

The authors are grateful to Joe Prospero, Richard Arimoto, Sangeeta Sharma, Zhouqing Xie and Rosie Chance for assisting in the retrieval of historical data. J. C. G. M. acknowledges financial support from the State Agency for Research of the Spanish MCIU through the "Center of Excellence Severo Ochoa" award to the Instituto de Astrofísica de Andalucía (SEV-2017-0709) and the Ramon y Cajal Program (RYC-2016-19570). A.S.-L. acknowledges financial support from the European Research Council Executive Agency under the European Union's Horizon 2020 Research and Innovation programme (Project 'ERC-2016-COG 726349 CLIMAHAL'). R. P. F. would like to thank financial support from ANPCyT (PICT 2015-0714), UNCuyo (SeCTyP M032/3853) and UTN (PID 4920-194/2018).

References

- Allan, J. D., et al. (2009), Composition and properties of atmospheric particles in the eastern Atlantic and impacts on gas phase uptake rates, *Atmos. Chem. Phys.*, 9(23), 9299-9314, doi: 10.5194/acp-9-9299-2009.
- Arimoto, R., R. A. Duce, and B. J. Ray (1989), Concentration, Sources and Air-Sea Exchange of Trace Elements in the Atmosphere over the Pacific Ocean, in *SEAREX: The Sea/Air Exchange Program*, edited by J. P. Riley and R. Chester, Academic Press, London, UK.

- Arimoto, R., R. A. Duce, B. J. Ray, A. D. Hewitt, and J. Williams (1987), Trace elements in the atmosphere of American Samoa: Concentrations and deposition to the tropical South Pacific, *J. Geophys. Res. [Atmos.]*, 92(D7), 8465-8479, doi: 10.1029/JD092iD07p08465.
- Arimoto, R., B. J. Ray, R. A. Duce, A. D. Hewitt, R. Boldi, and A. Hudson (1990), Concentrations, sources, and fluxes of trace elements in the remote marine atmosphere of New Zealand, *J. Geophys. Res. [Atmos.]*, 95(D13), 22389-22405, doi: 10.1029/JD095iD13p22389.
- Arimoto, R., R. A. Duce, B. J. Ray, W. G. Ellis Jr., J. D. Cullen, and J. T. Merrill (1995), Trace elements in the atmosphere over the North Atlantic, *J. Geophys. Res. [Atmos.]*, 100(D1), 1199-1213, doi: 10.1029/94jd02618.
- Arimoto, R., R. A. Duce, D. L. Savoie, J. M. Prospero, R. Talbot, J. D. Cullen, U. Tomza, N. F. Lewis, and B. J. Ray (1996), Relationships among aerosol constituents from Asia and the North Pacific during PEM-West A, *J. Geophys. Res. [Atmos.]*, 101(D1), 2011-2023, doi: 10.1029/95jd01071.
- Baker, A. R. (2004), Inorganic iodine speciation in tropical Atlantic aerosol, *Geophys. Res. Lett.*, 31(23), doi: 10.1029/2004gl020144.
- Baker, A. R. (2005), Marine Aerosol Iodine Chemistry: The Importance of Soluble Organic Iodine, *Environ. Chem.*, 2(4), 295-298, doi: <https://doi.org/10.1071/EN05070>.
- Baker, A. R., D. Thompson, M. L. A. M. Campos, S. J. Parry, and T. D. Jickells (2000), Iodine concentration and availability in atmospheric aerosol, *Atmos. Environ.*, 34(25), 4331-4336, doi: [https://doi.org/10.1016/S1352-2310\(00\)00208-9](https://doi.org/10.1016/S1352-2310(00)00208-9).
- Barrie, L. A., and M. J. Barrie (1990), Chemical components of lower tropospheric aerosols in the high arctic: Six years of observations, *J. Atmos. Chem.*, 11(3), 211-226, doi: 10.1007/bf00118349.
- Barrie, L. A., R. Staebler, D. Toom, B. Georgi, G. den Hartog, S. Landsberger, and D. Wu (1994), Arctic aerosol size-segregated chemical observations in relation to ozone depletion during Polar Sunrise Experiment 1992, *J. Geophys. Res. [Atmos.]*, 99(D12), 25439-25451, doi: 10.1029/94jd01514.
- Carpenter, L. J., S. M. MacDonald, M. D. Shaw, R. Kumar, R. W. Saunders, R. Parthipan, J. Wilson, and J. M. C. Plane (2013), Atmospheric iodine levels influenced by sea surface emissions of inorganic iodine, *Nat. Geosci.*, 6(2), 108-111, doi: 10.1038/ngeo1687.
- Chance, R. J., et al. (2019), Global sea-surface iodide observations, 1967–2018, *Scientific Data*, 6(1), 286, doi: 10.1038/s41597-019-0288-y.
- Cheng, Z. L., K. S. Lam, L. Y. Chan, T. Wang, and K. K. Cheng (2000), Chemical characteristics of aerosols at coastal station in Hong Kong. I. Seasonal variation of major ions, halogens and mineral dusts between 1995 and 1996, *Atmos. Environ.*, 34(17), 2771-2783, doi: [https://doi.org/10.1016/S1352-2310\(99\)00343-X](https://doi.org/10.1016/S1352-2310(99)00343-X).
- Cuevas, C. A., et al. (2018), Rapid increase in atmospheric iodine levels in the North Atlantic since the mid-20th century, *Nat. Commun.*, 9(1), 1452, doi: 10.1038/s41467-018-03756-1.
- Droste, E. (2017), Soluble Iodine Speciation in Indian Ocean Aerosols and its Impact on Marine Boundary Layer Chemistry, Wageningen University (NE) and University of East Anglia (UK).
- Duce, R. A., J. W. Winchester, and T. W. Van Nahl (1965), Iodine, bromine, and chlorine in the Hawaiian marine atmosphere, *J. Geophys. Res.*, 70(8), 1775-1799, doi: 10.1029/JZ070i008p01775.
- Duce, R. A., J. W. Winchester, and T. W. Van Nahl (1966), Iodine, bromine, and chlorine in winter aerosols and snow from Barrow, Alaska, *Tellus*, 18(2-3), 238-248, doi: 10.1111/j.2153-3490.1966.tb00232.x.
- Duce, R. A., A. H. Woodcock, and J. L. Moyers (1967), Variation of ion ratios with size among particles in tropical oceanic air1, *Tellus*, 19(3), 369-379, doi: 10.1111/j.2153-3490.1967.tb01492.x.
- Duce, R. A., W. H. Zoller, and J. L. Moyers (1973), Particulate and gaseous halogens in the Antarctic atmosphere, *J. Geophys. Res.*, 78(33), 7802-7811, doi: 10.1029/JC078i033p07802.
- Duce, R. A., R. Arimoto, B. J. Ray, C. K. Unni, and P. J. Harder (1983), Atmospheric trace elements at Enewetak Atoll: 1. Concentrations, sources, and temporal variability, *J. Geophys. Res. [Oceans]*, 88(C9), 5321-5342, doi: 10.1029/JC088iC09p05321.
- Fernandez, R. P., R. J. Salawitch, D. E. Kinnison, J. F. Lamarque, and A. Saiz-Lopez (2014), Bromine partitioning in the tropical tropopause layer: implications for stratospheric injection, *Atmos. Chem. Phys.*, 14(24), 13391-13410, doi: 10.5194/acp-14-13391-2014.
- Fernandez, R. P., A. Carmona-Balea, C. A. Cuevas, J. A. Barrera, D. E. Kinnison, J.-F. Lamarque, C. Blaszcak-Boxe, K. Kim, W. Choi, T. Hay, A.-M. Blechschmidt, A. Schönhardt, J. P. Burrows, and A. Saiz-Lopez (2019), Modeling the Sources and Chemistry of Polar Tropospheric Halogens (Cl, Br, and I) Using the CAM-Chem Global Chemistry-Climate Model, *J. Adv. Model Earth Sy.*, 11(7), 2259-2289, doi: <https://doi.org/10.1029/2019MS001655>.
- Frieß, U., T. Deutschmann, B. S. Gilfedder, R. Weller, and U. Platt (2010), Iodine monoxide in the Antarctic snowpack, *Atmos. Chem. Phys.*, 10(5), 2439-2456, doi: 10.5194/acp-10-2439-2010.

- Gäbler, H.-E., and K. G. Heumann (1993), Determination of atmospheric iodine species using a system of specifically prepared filters and IDMS, *Fresenius J. Anal. Chem.*, 345(1), 53-59, doi: 10.1007/bf00323326.
- Garland, J. A., and H. Curtis (1981), Emission of iodine from the sea surface in the presence of ozone, *J. Geophys. Res. [Oceans]*, 86(C4), 3183-3186, doi: 10.1029/JC086iC04p03183.
- Gilfedder, B. S., M. Petri, and H. Biester (2007), Iodine and bromine speciation in snow and the effect of orographically induced precipitation, *Atmos. Chem. Phys.*, 7(10), 2661-2669, doi: 10.5194/acp-7-2661-2007.
- Gilfedder, B. S., S. C. Lai, M. Petri, H. Biester, and T. Hoffmann (2008), Iodine speciation in rain, snow and aerosols, *Atmos. Chem. Phys.*, 8(20), 6069-6084, doi: 10.5194/acp-8-6069-2008.
- Gilfedder, B. S., R. Chance, U. Dettmann, S. C. Lai, and A. R. Baker (2010), Determination of total and non-water soluble iodine in atmospheric aerosols by thermal extraction and spectrometric detection (TESI), *Anal. Bioanal. Chem.*, 398(1), 519-526, doi: 10.1007/s00216-010-3923-1.
- Hirofumi, T., H. Hiroshi, I. Kiyoshi, and Y. Noboru (1987), The Iodine Content of Atmospheric Aerosols as Determined by the Use of a Fluoropore Filter® for Collection, *Bull. Chem. Soc. Jpn.*, 60(9), 3195-3198, doi: 10.1246/bcsj.60.3195.
- Huang, S., R. Arimoto, and K. A. Rahn (2001), Sources and source variations for aerosol at Mace Head, Ireland, *Atmos. Environ.*, 35(8), 1421-1437, doi: [https://doi.org/10.1016/S1352-2310\(00\)00368-X](https://doi.org/10.1016/S1352-2310(00)00368-X).
- Jalkanen, L., and P. Manninen (1996), Multivariate data analysis of aerosols collected on the Gulf of Finland, *Environmetrics*, 7(1), 27-38, doi: 10.1002/(sici)1099-095x(199601)7:1<27::aid-env159>3.0.co;2-3.
- Kang, H., S. Xu, X. Yu, B. Li, W. Liu, H. Yang, and Z. Xie (2015), Iodine speciation in aerosol particle samples collected over the sea between offshore China and the Arctic Ocean, *Adv. Polar Sci.*, 26(3), 215-221, doi: 10.13679/j.advps.2015.3.00215.
- Koenig, T. K., S. Baidar, P. Campuzano-Jost, C. A. Cuevas, B. Dix, R. P. Fernandez, H. Guo, S. R. Hall, D. Kinnison, B. A. Nault, K. Ullmann, J. L. Jimenez, A. Saiz-Lopez, and R. Volkamer (2020), Quantitative detection of iodine in the stratosphere, *Proc. Natl. Acad. Sci.*, 117(4), 1860, doi: 10.1073/pnas.1916828117.
- Lai, S. C. (2008), Iodine Speciation in Atmospheric Aerosols in the Marine Boundary Layer, University Johannes Gutenberg Mainz, Mainz, Germany.
- Lai, S. C., T. Hoffmann, and Z. Q. Xie (2008), Iodine speciation in marine aerosols along a 30,000 km round-trip cruise path from Shanghai, China to Prydz Bay, Antarctica, *Geophys. Res. Lett.*, 35(21), doi: 10.1029/2008GL035492.
- Lai, S. C., J. Williams, S. R. Arnold, E. L. Atlas, S. Gebhardt, and T. Hoffmann (2011), Iodine containing species in the remote marine boundary layer: A link to oceanic phytoplankton, *Geophys. Res. Lett.*, 38(20), doi: 10.1029/2011gl049035.
- Lin, C. T., T. D. Jickells, A. R. Baker, A. Marca, and M. T. Johnson (2016), Aerosol isotopic ammonium signatures over the remote Atlantic Ocean, *Atmos. Environ.*, 133, 165-169, doi: <https://doi.org/10.1016/j.atmosenv.2016.03.020>.
- Lininger, R. L., R. A. Duce, J. W. Winchester, and W. R. Matson (1966), Chlorine, bromine, iodine, and lead in aerosols from Cambridge, Massachusetts, *J. Geophys. Res.*, 71(10), 2457-2463, doi: 10.1029/JZ071i010p02457.
- MacDonald, S. M., J. C. Gómez Martín, R. Chance, S. Warriner, A. Saiz-Lopez, L. J. Carpenter, and J. M. C. Plane (2014), A laboratory characterisation of inorganic iodine emissions from the sea surface: dependence on oceanic variables and parameterisation for global modelling, *Atmos. Chem. Phys.*, 14(11), 5841-5852, doi: 10.5194/acp-14-5841-2014.
- Magi, L., F. Schweitzer, C. Pallares, S. Cherif, P. Mirabel, and C. George (1997), Investigation of the Uptake Rate of Ozone and Methyl Hydroperoxide by Water Surfaces, *J. Phys. Chem. A*, 101(27), 4943-4949, doi: 10.1021/jp970646m.
- Martino, M., D. Hamilton, A. R. Baker, T. D. Jickells, T. Bromley, Y. Nojiri, B. Quack, and P. W. Boyd (2014), Western Pacific atmospheric nutrient deposition fluxes, their impact on surface ocean productivity, *Global Biogeochem. Cycles*, 28(7), 712-728, doi: <https://doi.org/10.1002/2013GB004794>.
- Miyake, Y., and S. Tsunogai (1963), Evaporation of iodine from the ocean, *J. Geophys. Res.*, 68(13), 3989-3993, doi: 10.1029/JZ068i013p03989.
- Moyers, J. L., and R. A. Duce (1972), Gaseous and particulate iodine in the marine atmosphere, *J. Geophys. Res.*, 77(27), 5229-5238, doi: 10.1029/JC077i027p05229.
- Moyers, J. L., and R. A. Duce (1974), The collection and determination of atmospheric gaseous bromine and iodine, *Anal. Chim. Acta*, 69(1), 117-127, doi: [https://doi.org/10.1016/0003-2670\(74\)80015-2](https://doi.org/10.1016/0003-2670(74)80015-2).
- O'Dowd, C., C. Monahan, and M. Dall'Osto (2010), On the occurrence of open ocean particle production and growth events, *Geophys. Res. Lett.*, 37(19), doi: <https://doi.org/10.1029/2010GL044679>.

- O'Dowd, C. D., J. L. Jimenez, R. Bahreini, R. C. Flagan, J. H. Seinfeld, K. Hämeri, L. Pirjola, M. Kulmala, S. G. Jennings, and T. Hoffmann (2002), Marine aerosol formation from biogenic iodine emissions, *Nature*, *417*(6889), 632-636, doi: 10.1038/nature00775.
- Ordóñez, C., J. F. Lamarque, S. Tilmes, D. E. Kinnison, E. L. Atlas, D. R. Blake, G. Sousa Santos, G. Brasseur, and A. Saiz-Lopez (2012), Bromine and iodine chemistry in a global chemistry-climate model: description and evaluation of very short-lived oceanic sources, *Atmos. Chem. Phys.*, *12*(3), 1423-1447, doi: 10.5194/acp-12-1423-2012.
- Paton-Walsh, C., et al. (2017), The MUMBA campaign: measurements of urban, marine and biogenic air, *Earth Syst. Sci. Data*, *9*(1), 349-362, doi: 10.5194/essd-9-349-2017.
- Pechtl, S., G. Schmitz, and R. von Glasow (2007), Modelling iodide – iodate speciation in atmospheric aerosol: Contributions of inorganic and organic iodine chemistry, *Atmos. Chem. Phys.*, *7*(5), 1381-1393, doi: 10.5194/acp-7-1381-2007.
- Prados-Roman, C., C. A. Cuevas, R. P. Fernandez, D. E. Kinnison, J. F. Lamarque, and A. Saiz-Lopez (2015a), A negative feedback between anthropogenic ozone pollution and enhanced ocean emissions of iodine, *Atmos. Chem. Phys.*, *15*(4), 2215-2224, doi: 10.5194/acp-15-2215-2015.
- Prados-Roman, C., C. A. Cuevas, T. Hay, R. P. Fernandez, A. S. Mahajan, S. J. Royer, M. Galí, R. Simó, J. Dachs, K. Großmann, D. E. Kinnison, J. F. Lamarque, and A. Saiz-Lopez (2015b), Iodine oxide in the global marine boundary layer, *Atmos. Chem. Phys.*, *15*(2), 583-593, doi: 10.5194/acp-15-583-2015.
- Rancher, J., and M. A. Kritz (1980), Diurnal fluctuations of Br and I in the tropical marine atmosphere, *J. Geophys. Res. [Oceans]*, *85*(C10), 5581-5587, doi: 10.1029/JC085iC10p05581.
- Saiz-Lopez, A., A. S. Mahajan, R. A. Salmon, S. J.-B. Bauguittie, A. E. Jones, H. K. Roscoe, and J. M. C. Plane (2007), Boundary Layer Halogens in Coastal Antarctica, *Science*, *317*(5836), 348-351, doi: 10.1126/science.1141408.
- Saiz-Lopez, A., R. P. Fernandez, C. Ordóñez, D. E. Kinnison, J. C. Gómez Martín, J. F. Lamarque, and S. Tilmes (2014), Iodine chemistry in the troposphere and its effect on ozone, *Atmos. Chem. Phys.*, *14*(23), 13119-13143, doi: 10.5194/acp-14-13119-2014.
- Saiz-Lopez, A., J. M. C. Plane, A. R. Baker, L. J. Carpenter, R. von Glasow, J. C. Gómez Martín, G. McFiggans, and R. W. Saunders (2012a), Atmospheric Chemistry of Iodine, *Chem. Rev.*, *112*(3), 1773-1804, doi: 10.1021/cr200029u.
- Saiz-Lopez, A., S. Baidar, C. A. Cuevas, T. K. Koenig, R. P. Fernandez, B. Dix, D. E. Kinnison, J.-F. Lamarque, X. Rodriguez-Lloveras, T. L. Campos, and R. Volkamer (2015), Injection of iodine to the stratosphere, *Geophys. Res. Lett.*, *42*(16), 6852-6859, doi: 10.1002/2015gl064796.
- Saiz-Lopez, A., et al. (2012b), Estimating the climate significance of halogen-driven ozone loss in the tropical marine troposphere, *Atmos. Chem. Phys.*, *12*(9), 3939-3949, doi: 10.5194/acp-12-3939-2012.
- Sharma, S., L. A. Barrie, E. Magnusson, G. Brattström, W. R. Leitch, A. Steffen, and S. Landsberger (2019), A Factor and Trends Analysis of Multidecadal Lower Tropospheric Observations of Arctic Aerosol Composition, Black Carbon, Ozone, and Mercury at Alert, Canada, *J. Geophys. Res. [Atmos.]*, *124*(24), 14133-14161, doi: 10.1029/2019jd030844.
- Sherwen, T. M., M. J. Evans, D. V. Spracklen, L. J. Carpenter, R. Chance, A. R. Baker, J. A. Schmidt, and T. J. Breider (2016a), Global modeling of tropospheric iodine aerosol, *Geophys. Res. Lett.*, *43*(18), 10012-10019, doi: 10.1002/2016gl070062.
- Sherwen, T. M., M. J. Evans, L. J. Carpenter, S. J. Andrews, R. T. Lidster, B. Dix, T. K. Koenig, R. Sinreich, I. Ortega, R. Volkamer, A. Saiz-Lopez, C. Prados-Roman, A. S. Mahajan, and C. Ordóñez (2016b), Iodine's impact on tropospheric oxidants: a global model study in GEOS-Chem, *Atmos. Chem. Phys.*, *16*(2), 1161-1186, doi: 10.5194/acp-16-1161-2016.
- Spolaor, A., et al. (2014), Seasonality of halogen deposition in polar snow and ice, *Atmos. Chem. Phys.*, *14*(18), 9613-9622, doi: 10.5194/acp-14-9613-2014.
- Sturges, W. T., and L. A. Barrie (1988), Chlorine, Bromine and Iodine in arctic aerosols, *Atmos. Environ.* (1967), *22*(6), 1179-1194, doi: https://doi.org/10.1016/0004-6981(88)90349-6.
- Thompson, A. M., J. C. Witte, S. J. Oltmans, F. J. Schmidlin, J. A. Logan, M. Fujiwara, V. W. J. H. Kirchhoff, F. Posny, G. J. R. Coetzee, B. Hoegger, S. Kawakami, T. Ogawa, J. P. F. Fortuin, and H. M. Kelder (2003), Southern Hemisphere Additional Ozonesondes (SHADOZ) 1998–2000 tropical ozone climatology 2. Tropospheric variability and the zonal wave-one, *J. Geophys. Res. [Atmos.]*, *108*(D2), doi: 10.1029/2002jd002241.
- Tilmes, S., et al. (2016), Representation of the Community Earth System Model (CESM1) CAM4-chem within the Chemistry-Climate Model Initiative (CCMI), *Geosci. Model Dev.*, *9*(5), 1853-1890, doi: 10.5194/gmd-9-1853-2016.
- Vogt, R., R. Sander, R. von Glasow, and P. J. Crutzen (1999), Iodine Chemistry and its Role in Halogen Activation and Ozone Loss in the Marine Boundary Layer: A Model Study, *J. Atmos. Chem.*, *32*(3), 375-395, doi: 10.1023/a:1006179901037.

- Weller, R., J. Wöltjen, C. Piel, R. Resenberg, D. Wagenbach, G. König-Langlo, and M. Kriews (2008), Seasonal variability of crustal and marine trace elements in the aerosol at Neumayer station, Antarctica, *Tellus B*, 60(5), 742-752, doi: 10.1111/j.1600-0889.2008.00372.x.
- Whitehead, D. C. (1984), The distribution and transformations of iodine in the environment, *Environ. Int.*, 10(4), 321-339, doi: 10.1016/0160-4120(84)90139-9.
- Wimschneider, A., and K. G. Heumann (1995), Iodine speciation in size fractionated atmospheric particles by isotope dilution mass spectrometry, *Fresenius J. Anal. Chem.*, 353(2), 191-196, doi: 10.1007/bf00322957.
- Xu, S., Z. Xie, B. Li, W. Liu, L. Sun, H. Kang, H. Yang, and P. Zhang (2010), Iodine speciation in marine aerosols along a 15000-km round-trip cruise path from Shanghai, China, to the Arctic Ocean, *Environ. Chem.*, 7(5), 406-412, doi: 10.1071/EN10048.
- Yodle, C. (2015), Iodine Speciation in Marine Aerosol, University of East Anglia (UK).
- Yodle, C., and A. R. Baker (2019), Influence of collection substrate and extraction method on the speciation of soluble iodine in atmospheric aerosols, *Atmos. Environ. X*, 1, 100009, doi: 10.1016/j.aeaoa.2019.100009.
- Yoshida, S., and Y. Muramatsu (1995), Determination of organic, inorganic and particulate iodine in the coastal atmosphere of Japan, *J. Radioanal. Nucl. Chem.*, 196(2), 295-302, doi: 10.1007/bf02038047.
- Yu, H., L. Ren, X. Huang, M. Xie, J. He, and H. Xiao (2019), Iodine speciation and size distribution in ambient aerosols at a coastal new particle formation hotspot in China, *Atmos. Chem. Phys.*, 19(6), 4025-4039, doi: 10.5194/acp-19-4025-2019.
- Zhang, L., X. Hou, and S. Xu (2016), Speciation of ¹²⁷I and ¹²⁹I in atmospheric aerosols at Risø, Denmark: insight into sources of iodine isotopes and their species transformations, *Atmos. Chem. Phys.*, 16(4), 1971-1985, doi: 10.5194/acp-16-1971-2016.
- Zieman, J. J., J. L. Holmes, D. Connor, C. R. Jensen, W. H. Zoller, D. M. Hermann, J. R. Parrington, and G. E. Gordon (1995), Atmospheric aerosol trace element chemistry at Mauna Loa Observatory: 1. 1979–1985, *J. Geophys. Res. [Atmos.]*, 100(D12), 25979-25994, doi: 10.1029/93jd03316.